Funded by the European Union

HORIZON EUROPE
EUROPEAN HEALTH AND DIGITAL; EXECUTIVE AGENCY (HADEA)

MADE-3D

Multi-Material Design using 3D Printing

Starting date of the project: 01/01/2023
Duration: 42 months

= Deliverable D2.2 =

Building and application of microscale simulation

Due Date: 31/12/2023
Date Submitted: 08/12/2023
Responsible WPL: John Aristeidakis (QTE)
Responsible TL: ROUX Guilhem (CEA)
Version: 1.1

Dissemination level		
P	Public	x
SEN	Sensitive, limited under the conditions of the Grant Agreement	
Classified R-UE/EU-R	EU RESTRICTED under the Commission Decision No2015/444	
Classified C-UE/EU-C	EU CONFIDENTIAL under the Commission Decision No2015/444	
Classified S-UE/EU-S	EU SECRET under the Commission Decision No2015/444	

This project has received funding from the European Union's Horizon Europe research and innovation program under grant agreement No 101091911.
Views and opinions expressed are those of the author(s) only and do not necessarily reflect those of the European Union or European Commission. Neither the European Union nor the granting authority can be held responsible for them.

AUTHOR

Author	Organization	Contact (e-mail, phone)
ROUX Guilhem	CEA	Guilhem.roux@cea.fr

DOCUMENT CONTROL

Document version	Date	Change
V0.1	27/11/2023	First draft
V1	07/12/2023	First version
V1.1	08/12/2023	Final version

VALIDATION

Reviewers	Name	Validation date
Work Package Leader	Aristeidakis John	27/11/2023
Project Manager	Marina de Souza Faria	07/12/2023
Project Coordinator	Dennis Lehnert	08/12/2023

Executive Summary

This report explains in details finite element thermomechanical model built to simulate monomaterial and bimaterial L-PBF (Laser Powder Bed Fusion) process at microscale and mesoscale. All equations for thermal and mechanical behavior are explained, as all boundary conditions and loading induced by the process. This model has been built using in-house finite element software.

The model has been used to simulate different generic cases, waiting more detailed process parameters. These cases are:

- Microscopic scale with one track simulation (for AlSi10Mg)
- Mesoscopic scale with up to ten coincident tracks and layers for monomaterial configuration (for AlS10iMg)
- Same with bimaterial configuration

Thermal and mechanical field obtained permits to define the geometry scale to be considered to achieve representativeness of thermal history and residual stresses. First simulation with bimaterial configuration show a very complex stress generation at interface wich leads us to conclude on the importance of near interface lasing strategy as material consolidation order (A then B, B then A).

CONTENTS

1. Introduction

This deliverable is dedicated to microscale and mesoscale simulations of dissimilar L-PBF manufacturing (Laser Powder Bed Fusion). This work is realised in the frame of the WP2 of the project (Design & Modelling). This work package is subdivided in four tasks:

- Computational path planning for joining dissimilar materials by DED (T2.1)
- Baseline alloy modification for improved joining by PBF-LB (T2.2)
- FEM modelling of residual stresses, thermal history, melt pool temperatures at micro level scale (T2.3)
- Use Case component design and simulation (T2.4)

The first main topic of this workpackage is to define materials or materials assembly (in case of DED process) to optimise manufacturing reliability as part properties. The first difficulty induced by these two high temperature processes involving bimaterial manufacturing is to manage inter diffusion between both materials. Inter diffusion leads often to intermetallic precipitation. Generally, intermetallic phases are brittle. In the case of DED process, diffusion aspects can be controlled using intermediate layers. It is also the case for others bimaterial processes like brazing, HIP (High Isostatic Pressing, welding,…). For L-PBF process, the only solution is to choose a compatible chemical composition for both materials and limiting diffusion mechanism. This work is dedicated to first two tasks (T21 and T2.2).

If we want to optimise chemical compositions in L-PBF process in that way, we need to have an idea of the thermal history at interface between materials. Knowing this thermal history, we can be able to predict numerically inter diffusion zones at interface.

Another difficulty of these bimaterial processes are residual stresses. Residual stresses induced by material contraction during cooling, moreover with multimaterial processes inducing local thermal expansion mismatches (see **Figure 1**), is the main cause for small or large cracking in dissimilar material assemblies, and so by extrapolation to high temperature multimaterial 3D printing processes, whatever the process used (cold spray, L-PBF, DED, etc…). This cracking is of course also dependent on materials ductilities.

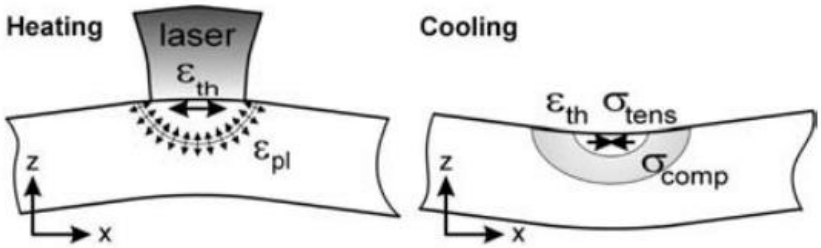

***Figure 1**: thermal gradient effect for monomaterial L-PBF process [1]*

As a result, we need to consider three different main aspects in our materials/process optimisation:

- Limitation of residual stresses induced by the process
- The best mechanical compatibility between both materials, i.e thermal expansion and ductility in first order
- The best chemical compatibility between materials, i.e. intermetallic precipitation.

The numerical tool which will be developed in this T2.3 work will permit the project to develop best materials couples and process parameters to achieve bimaterial parts with good mechanical properties. Results form with workpackage will be usefull for other tasks from this workpackage, as we need inputs form other workpackages. The interaction chart of this T2.3 is presented **Figure 2**.

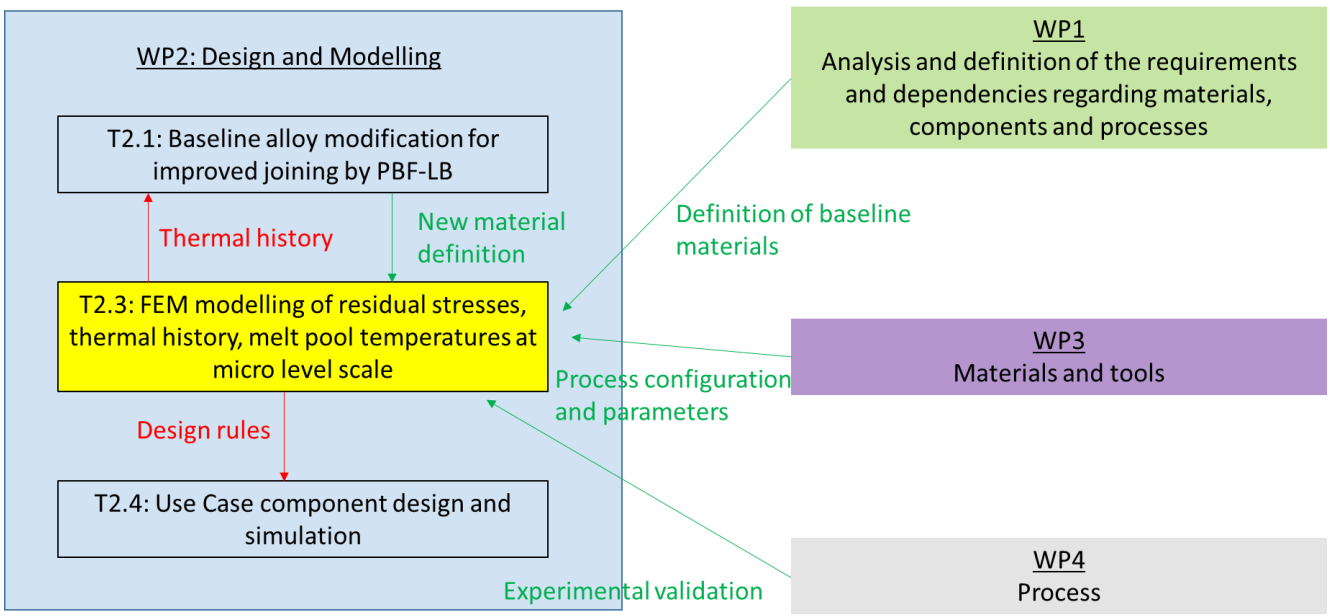

***Figure 2**: T2.3 interaction chart*

The last topic of this workpackage WP2 is dedicated to the design and optimisation of use cases using DED or L-PBF process (T2.4).

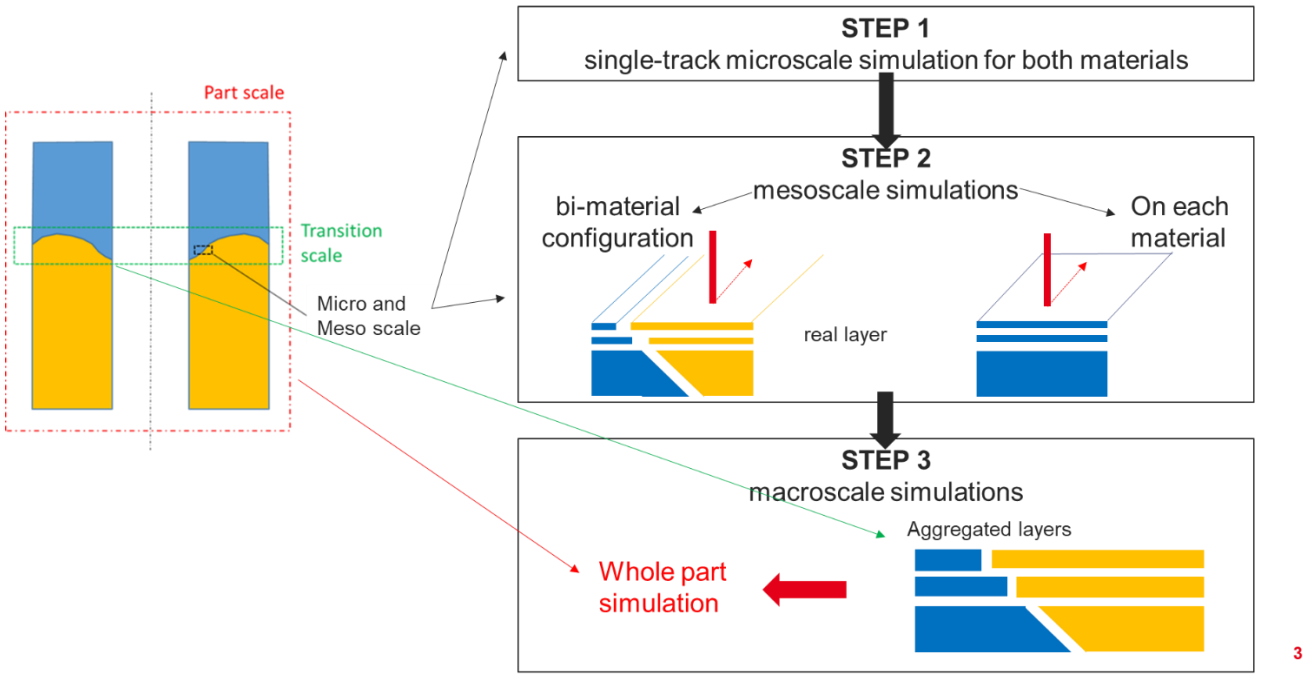

***Figure 3**: global simulation strategy*

During this project, we will focus our work on Copper/Aluminium L-PBF configuration, as it is the most challenging couple in terms of inter-diffusion and mechanical residuals stresses. More precisely, we will deal with AlSi10Mg/CuCrZr bimaterial configuration.

All the work realised during this first year as explanations on simulation strategy are given in APPENDIX A.

2. Results and Discussion

Before to go in details on simulation building and results, we present Figure 3 the global simulation strategy wich will be conducted during this project. Three simulation scales will be studied:

- **Microscale simulation**. We focus here on the study of a single track lasing. Main outputs at that scale are melt pool dimension. Melt pool dimension is very important for thermal history and residual stresses generation. At that scale, we can fit numerous thermal loading and boundary conditions involved in this process (see **Figure 4**) before going to upper scales, generally involving lot of more computation times.

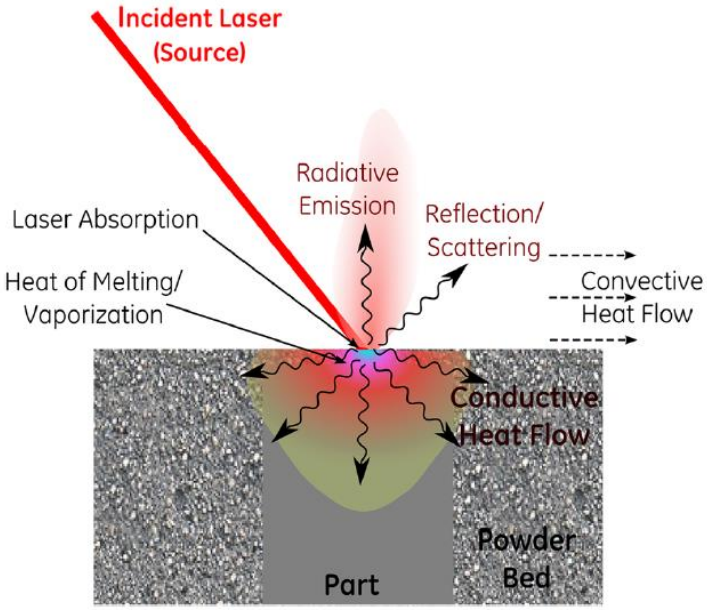

***Figure 4**: thermal model at micro scale [2]*

- **Mesoscale simulation**. At that scale, we deal with several contiguous lasing tracks and several layers. This scale permits to have a good access to thermo-mechanical phenomenoms acting during the process. At that scale we will introduce bimaterial L-PBF configuration. This scale will permit to extract proper thermal history for diffusion calculations and residuals stresses. Moreover, these simulation at that scale will permit to extract inherent strains ([3]) for macroscale simulations.

- **Macroscale simulation.** At that scale we will be able to compute simulation on whole parts. These simulations are needed to predict part deformation during process and in a certain way, induced stresses. Macroscale simulation building will be done during next year.

From this first year T2.2 work, we present in this deliverable:

- Building of base thermomechanical model with associated process thermal loading and boundary conditions.
- Microscale simulations with AlSI10Mg
- Monomaterial mesoscale simulation with AlSi10Mg
- Bimaterial mesoscale simulation with AlSi10Mg/CuCrZr

We focused on simulations on AlSi10Mg for model building, but similar simulations can be run using CuCrZr. As process parameters are not known at that time, there is no needs to conduce simulation for both materials.

2.1. Model building

For these simulations, we built a thermomechanical model (sequential iterative coupling) using in-house open source software (Cast3M **[4]**). Main things to consider for our L-PBF application are:

- Properly model all boundary conditions, in particular thermal ones (convection, radiation, laser source model)
- Manage powder behavior. Indeed, powder layer (see Figure 5) have a very low thermal conductivity and close to none mechanical rigidity.
- Include latent heat effects during solid/liquid phase change. It is a little bit tricky to integrate this phenomenon for high-speed liquefaction/solidification processes.

As bimaterial process parameters are not yet consolidated in terms of process parameters, we used process parameters from litterature.

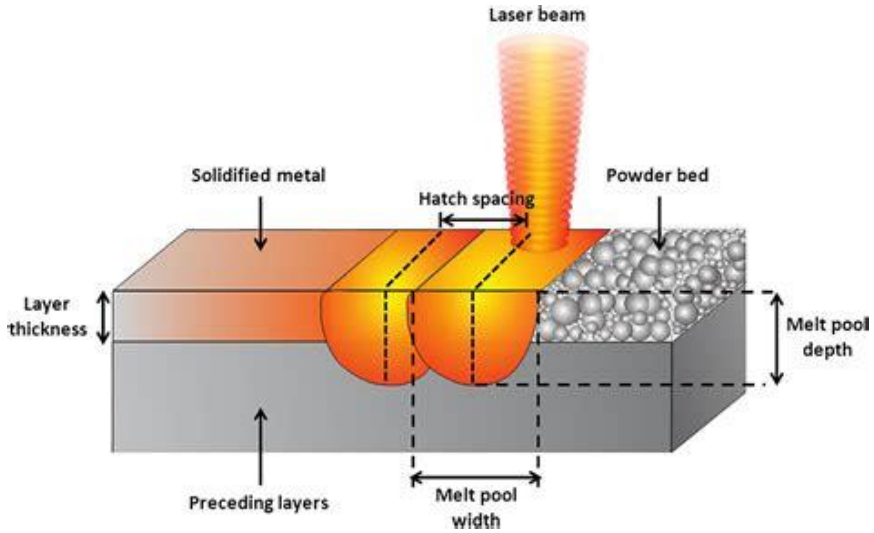

***Figure 5**: powder and bulk material configuration during L-PBF process [5]*

2.1. Single track simulation (AlSi10Mg)

We present **Figure 6** the temperature field obtained for AlSi10Mg. From this thermal information, we can compute melt pool size. Computed melt pool size is quite coherent with the one computed from classic analytical model using Rosenthal equation ([6]).

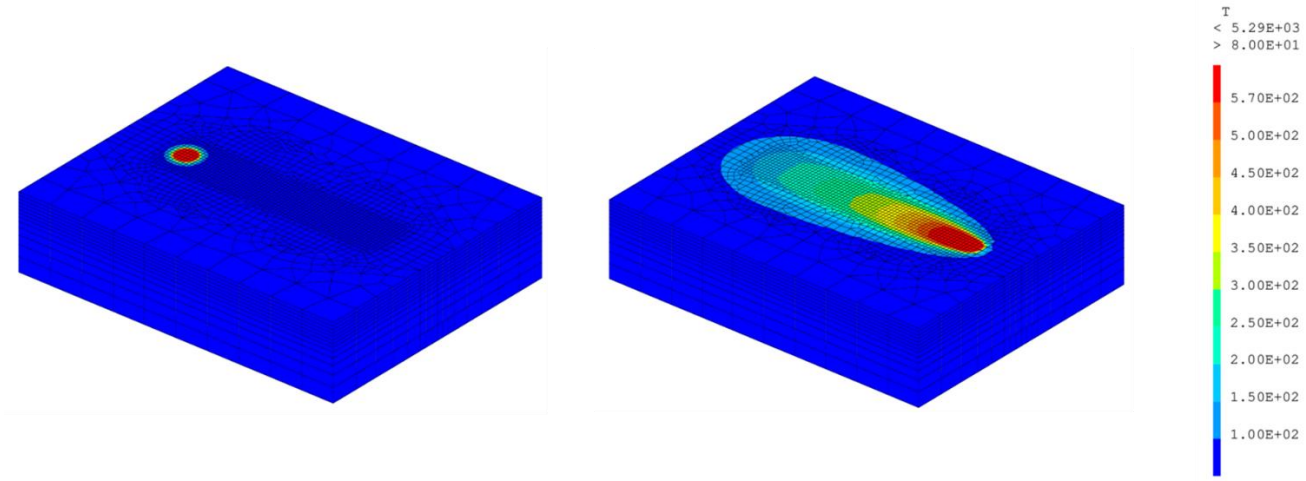

***Figure 6**: temperature during lasing of a single line (AlSi10Mg)*

For mechanical behavior materials, we choose in first step a simple perfectly plastic behavior depending on temperature. Residual stresses induced are mainly traction ones due to material contraction during cooling. We observe laser ignition and stop effect due to different thermal cooling speed at that points.

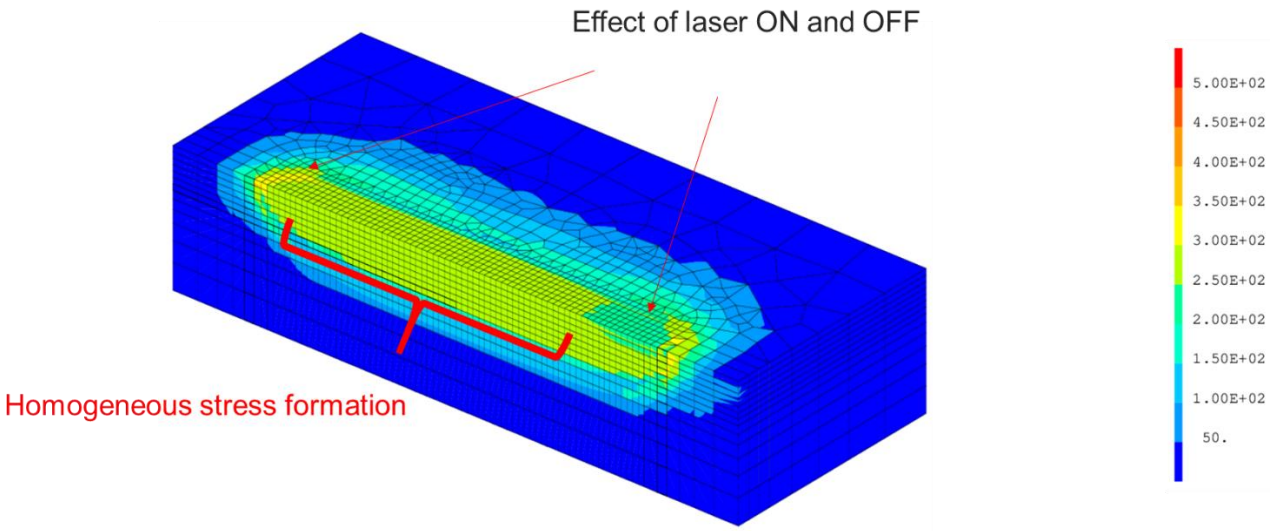

***Figure 7**: V.M. stress field during lasing of a single line (AlSi10Mg)*

Integrating more thermal non-linearities as properties depending on temperature and liquid conductivity change melt pool dimensions, but we pay the price in terms of computation times as seen **Table 1**. If computation time is not problematic for monotrack simulation, computations times are important (>1 day) for mesoscopic one when we compute several tracks/layers.

If we want to accelerate computation times, we can neglect non-linearities in a first approach. It makes sense for lasing strategy optimisation and various sensibility analysis.

							melt pool dimension		
N	**NL thermal properties**	**liquid conductivity**	**powder/bulk phase change**	**latent heat**	**time (min)**	**factor**	**length [µm]**	**width [µm]**	**depth [µm]**
1					10	1.00	*530*	*195*	*120*
2	x				30	2.94	*485*	*195*	*120*
3	x	x			89	8.79	*394*	*260*	*120*
4	x	x	x		93	9.19	*432*	*195*	*120*
5	x		x		39	3.90	*545*	*195*	*120*
6				x	41	4.05	*909*	*195*	*90*
7	x	x		x	269	26.66	*667*	*195*	*90*

***Table 1:** Evolution of melt pool dimensions and computation times depending on thermal non-linearities assumptions*

2.2. Mesoscopic monomaterial simulation (AlSi10Mg)

We conducted a mesoscopic simulation with five contiguous laser lines during five layers (total of 25 laser lines). We made here the assumption of a lasing strategy without rotation between layers Deep analysis of thermal evolution might lead us to conclude that scans with ten layers (10x10 laser lines) is necessary to achieve a kind of stable thermal periodicity (see **Figure 9**).

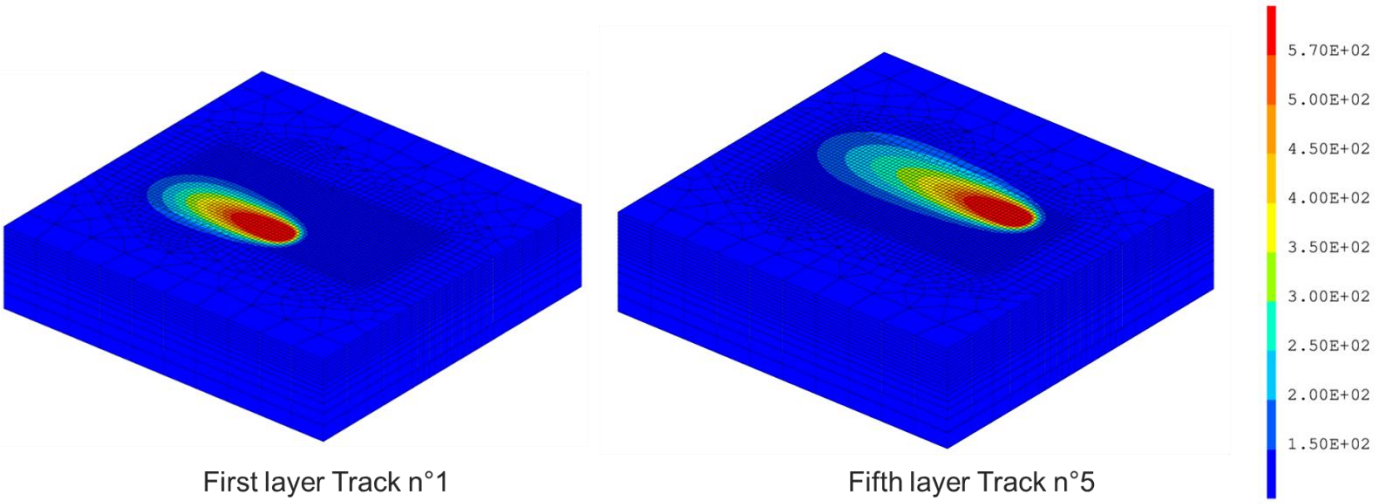

***Figure 8**: temperature field during first and last laser line for 5x5 mesoscopic simulation (AlSi10Mg)*

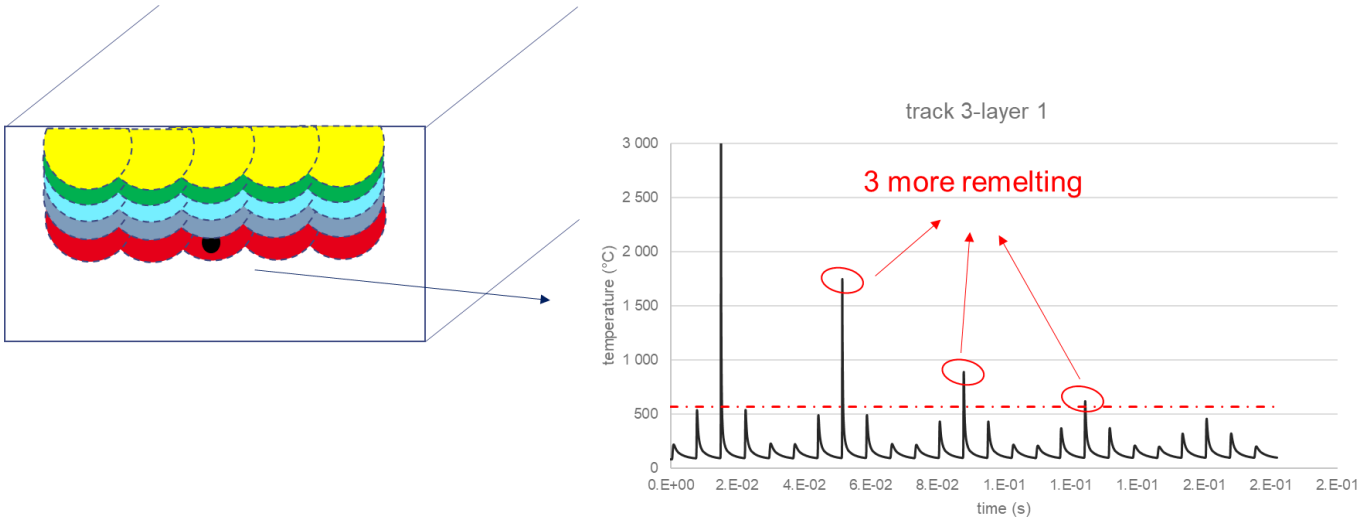

***Figure 9**: upper thermal history at third scan (AlSi10Mg)*

Concerning mechanical residual field, a quick stabilisation of stress field is observe with contiguous tracks is observed (**Figure 10**). Last two tracks present side effects. We observe a lower residual stresses zone below approximatively five manufactured layers, wich probably correspond to a kind of stress relieve phenomenon induced by medium temperatures without melting. Therefore, five layers is not sufficient if we want to quantify internal residuals stresses of our material. To quantify upper residual stresses wich are quantitatively more important, five layers seems sufficient.

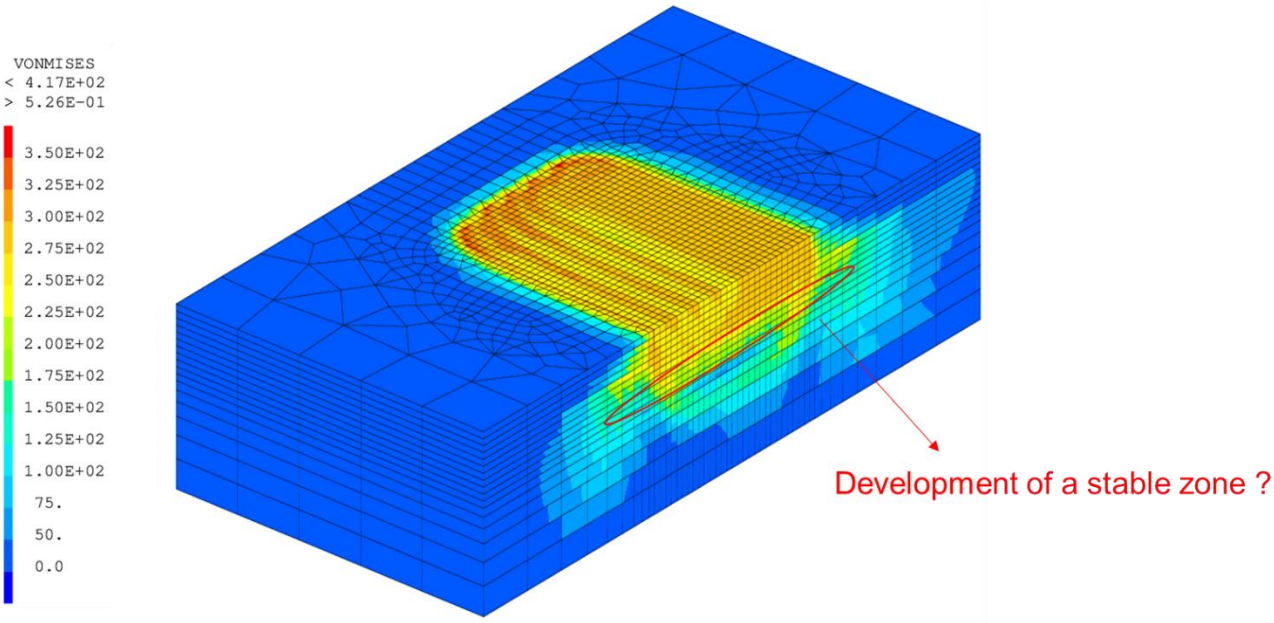

***Figure 10**: V.M. residual stress field at the end of last track of the fifth deposited layer (AlSi10Mg)*

Taking into account these preliminaries consideration, we successfully launched a 10x10 thermomechanical configuration. We can now really observe that we have a relative homogenous stress concentration in last fifth layers due to layer remelting. Below this zone, we observe a stress relieving do hight temperatures attempt (see **Figure 11**). This result is very important because that mean that for XR residual stresses measurements, as-built surface analysis (gauge depth of about 30-50µm) will give different results as inside material.

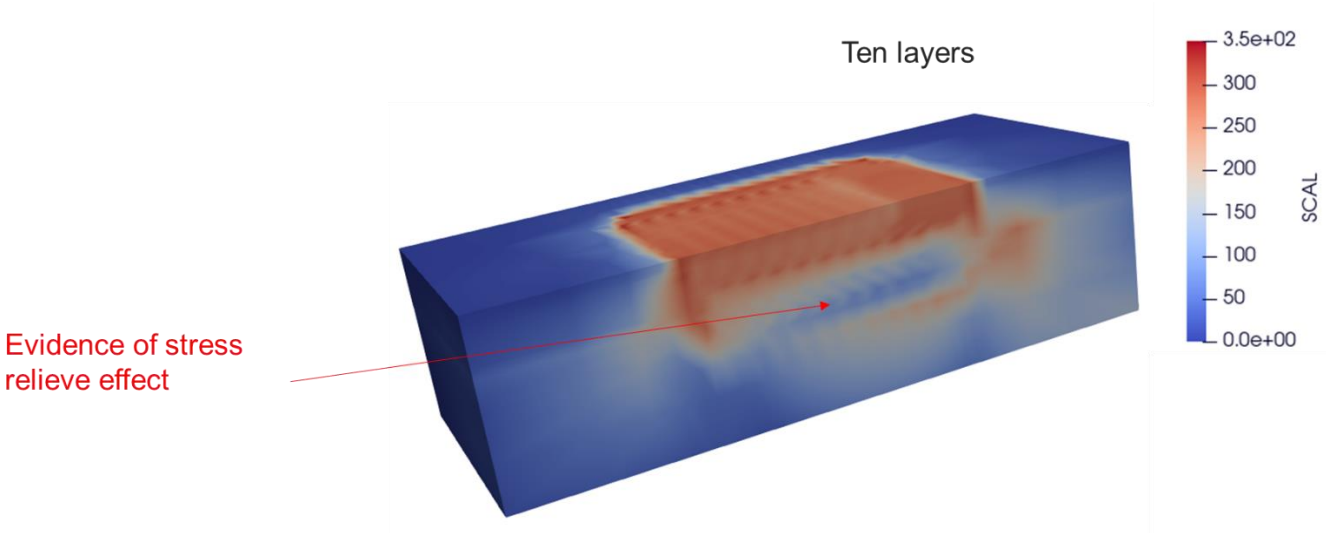

***Figure 11**: V.M. residual stress field at the end of last track for ten deposited layer (AlSi10Mg)*

2.3. Mesoscopic bimaterial simulation (AlSi10Mg/CuCrZr)

We simulated 5x5 bimaterial thermomechanical simulation for AlSi10Mg/CuCrZr couple. As expected, we obtain a complex residual stresses field with again two distinct zones which are near surface one (≈5 layers) and sub-surface one (<5 layers).

An example of thermal fields are given **Figure 12**. As material properties and lasing parameters are different between two materials, this induce complex thermal history at interface. These results can now be used to complete diffusion simulation at the interface. Near interface, bimaterial configuration induce more remelting as melt pool from one material can penetrate the other. That means that positions of the laser near interface has an important effect on residual stresses, as the order of consolidation between first and second material.

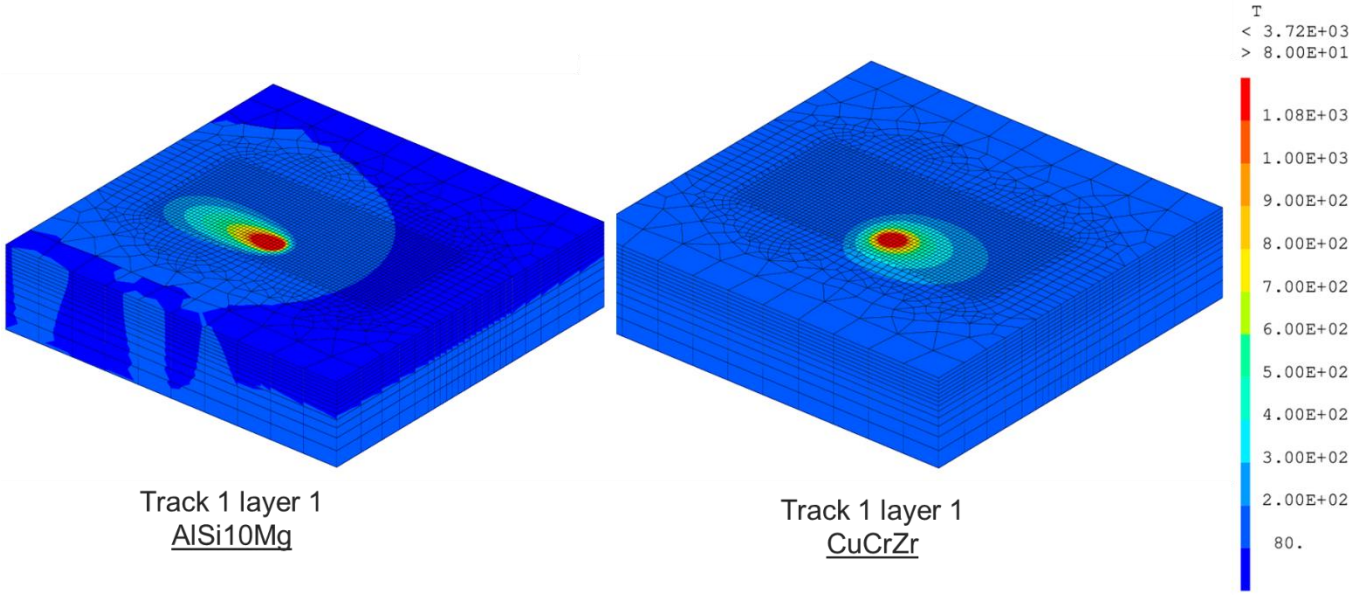

***Figure 12**: temperature field during first line for each material for 5x5 mesoscopic bimaterial simulation*

The presence of two materials with different thermal/mechanical properties generate highly complex residual stress field at interface, like we can see

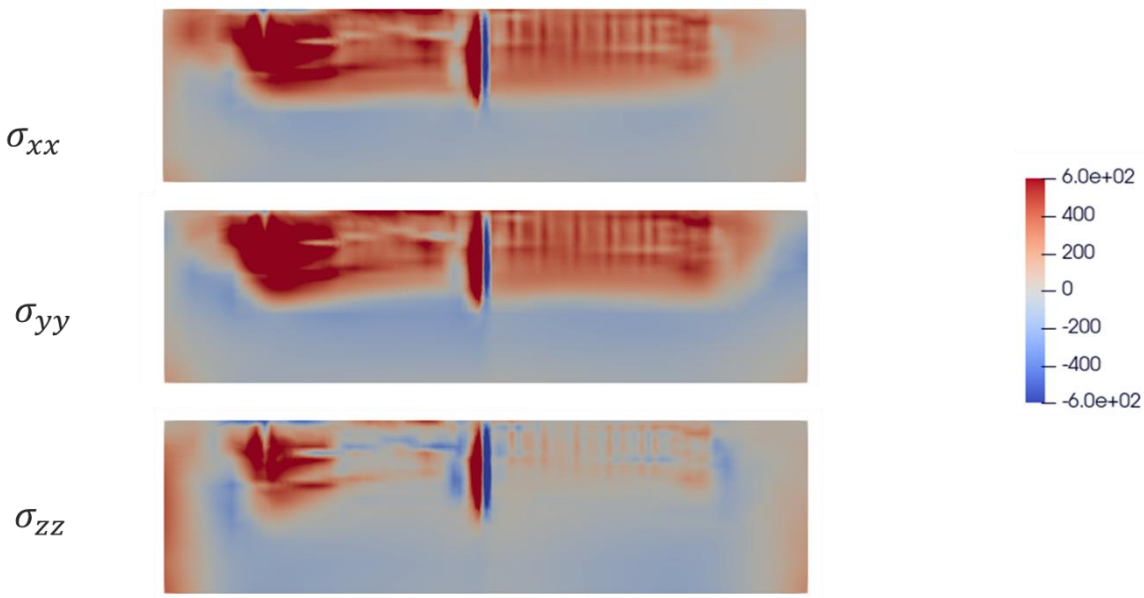

***Figure 13**: stress field along lasing direction for 5x5 mesoscopic bimaterial simulation*

3. Conclusion

During this first-year project period, we built a complete Finite Element thermomechanical model for mono and bimaterial L-PBF process at micro and meso-scale, including liquid/solid latent heat, powder to bulk evolutions as layer deposition.

Concerning thermal results, this model permit to access complete thermal history, in particular at interface for bimaterial configuration. These informations are usefull for diffusion calculations at interface. 10x10 tracks/layers seems to be sufficient to be representative.

For mechanical stresses generated by the process, we need less coincident tracks to be simulated (around four or five tracks). Computation of five deposited layers are sufficient to characterise near surface residual stresses. If we want to have an idea of inside material residual stresses, at least 10 layers will be needed.

In bimaterial configuration, complex residual stresses are observed near interface. As a result, order of material consolidation as lasing strategy are preponderant.

Thermal non-linearities consume a lot computation times. As thermal solver of our in-house code is not parallelized, computation times are quite long. A first work of next year will be to transfer models inside commercial F.E. software ANSYS©

4. Degree of Progress

All main tasks of this T2.3 WP are listed **Table 2**. According to first results presented in this report for this first year, we had a task consisting in building same model inside commercial F.E. ANSYS©.

Table 2: Progress table for tasks involved in T2.3 WP.

Deadline	sub-tasks	status	commentes
M12	thermal model	100%	
M12	mechanical model	90%	
M12	monotrack simulation on generic case	100%	done on AlSi10Mg and CuCrZr
M12	multilayer scan pattern on generic case	100%	done on AlSi10Mg
M12	Model building inside ANSYS©	20%	
M24	monotrack line simulation on real case	0%	wait process parameters from ICGV. Need to be done on both materials
M24	bimaterial multilayer scan pattern on real case	0%	wait process parameters from ICGV. Need to be done on both materials
M24	multilayer scan pattern on generic case	100%	done on a simplified case
M24	bimaterial multilayer scan pattern on real case	0%	wait process parameters from ICGV. Need to be done on both materials
M24	inherent strain tensor identification using mesoscopic simulations	0%	
M24	building of macroscopic simulation	0%	
M38	experimental validation on monomaterial process	0%	
M38	experimental validation on bimaterial process	0%	
M38	experimental/simulation comparaison		samples need to be defined (in progress with WP4)

5. References

[1] P. Mercelis, J. Kruth, Residual stresses in selective laser sintering and selective laser melting, Rapid Prototyp. J. 12 (2006) 254–265. https://doi.org/10.1108/13552540610707013.

[2] T.G. Spears, S.A. Gold, In-process sensing in selective laser melting (SLM) additive manufacturing, Integrating Mater. Manuf. Innov. 5 (2016) 16–40. https://doi.org/10.1186/s40192-016-0045-4.

[3] Ueda Y., Fukuda K., Tanigawa M., New Measuring Method of 3-Dimensional Residual Stresses Based on Theory of Inherent Strain, J. Soc. Nav. Archit. Jpn. 1979 (1979) 203–211. https://doi.org/10.2534/jjasnaoe1968.1979.203.

[4] Cast3M Code, (n.d.). http://www-cast3m.cea.fr/.

[5] A. Sola, A. Nouri, Microstructural porosity in additive manufacturing: The formation and detection of pores in metal parts fabricated by powder bed fusion, J. Adv. Manuf. Process. 1 (2019). https://doi.org/10.1002/amp2.10021.

[6] D. Rosenthal, Mathematical theory of heat distribution during welding and cutting, Weld. J. 20 (n.d.) 220–234.

[7] E. Soylemez, E. Koç, M. Coşkun, Thermo-mechanical simulations of selective laser melting for AlSi10Mg alloy to predict the part-scale deformations, Prog. Addit. Manuf. 4 (2019) 465–478. https://doi.org/10.1007/s40964-019-00096-4.

[8] N.E. Uzan, R. Shneck, O. Yeheskel, N. Frage, Fatigue of AlSi10Mg specimens fabricated by additive manufacturing selective laser melting (AM-SLM), Mater. Sci. Eng. A. 704 (2017) 229–237. https://doi.org/10.1016/j.msea.2017.08.027.

[9] A. Rausch, V. Küng, C. Pobel, M. Markl, C. Körner, Predictive Simulation of Process Windows for Powder Bed Fusion Additive Manufacturing: Influence of the Powder Bulk Density, Materials. 10 (2017) 1117. https://doi.org/10.3390/ma10101117.

[10] M. Ferraiuolo, V. Giannella, E. Armentani, R. Citarella, Numerical Investigation on the Service Life of a Liquid Rocket Engine Thrust Chamber, Metals. 13 (2023) 470. https://doi.org/10.3390/met13030470.

[11] N. Makoana, I. Yadroitsava, H. Möller, I. Yadroitsev, Characterization of 17-4PH Single Tracks Produced at Different Parametric Conditions towards Increased Productivity of LPBF Systems—The Effect of Laser Power and Spot Size Upscaling, Metals. 8 (2018) 475. https://doi.org/10.3390/met8070475.

[12] X.W. Zhang, Q.J. Wang, X. Zhou, B. Liang, Tensile behavior of high temperature Cu-Cr-Zr alloy:, in: Hong Kong, China, 2015. https://doi.org/10.2991/peee-15.2015.51.

[13] A. Ghasemi, E. Fereiduni, M. Balbaa, S.D. Jadhav, M. Elbestawi, S. Habibi, Influence of alloying elements on laser powder bed fusion processability of aluminum: A new insight into the oxidation tendency, Addit. Manuf. 46 (2021) 102145. https://doi.org/10.1016/j.addma.2021.102145.

[14] K. Zhang, E. Gaganidze, M. Gorley, Development of the material property handbook and database of CuCrZr, Fusion Eng. Des. 144 (2019) 148–153. https://doi.org/10.1016/j.fusengdes.2019.04.094.

[15] N. Tissot, Amélioration du procédé LBM par nanostructuration de poudres d'aluminium, Université de Lyon, 2019.

[16] J. Goldak, A. CHAKRAVARTI, M. BIBBY, A New Finite Element Model for Welding Heat Sources, Metall. Mater. Trans. B. 15 (1984) 299–305.

[17] G. Bugeda Miguel Cervera, G. Lombera, Numerical prediction of temperature and density distributions in selective laser sintering processes, Rapid Prototyp. J. 5 (1999) 21–26. https://doi.org/10.1108/13552549910251846.

[18] P. Promoppatum, S.-C. Yao, P.C. Pistorius, A.D. Rollett, A Comprehensive Comparison of the Analytical and Numerical Prediction of the Thermal History and Solidification Microstructure of Inconel 718 Products Made by Laser Powder-Bed Fusion, Engineering. 3 (2017) 685–694. https://doi.org/10.1016/J.ENG.2017.05.023.

[19] Y. Tang, G. Dong, Q. Zhou, Y.F. Zhao, Lattice Structure Design and Optimization With Additive Manufacturing Constraints, IEEE Trans. Autom. Sci. Eng. (2017) 1–17. https://doi.org/10.1109/TASE.2017.2685643.

[20] J. Wisniewski, J.-M. Drezet, D. Ayrault, B. Cauwe, Determination of the thermophysical properties of a CuCr1Zr alloy from liquid state down to room temperature, Int. J. Mater. Form. 1 (2008) 1059–1062. https://doi.org/10.1007/s12289-008-0201-2.

[21] D.K. Stefan, M.A. Rodriguez, D.R. Bradley, J. Griego, L. Deibler, J.M. Rodelas, J. Carroll, Thermal Characterization of AISI1ONlig Alloy Fabricated by Selective Laser Melting, in: Albuquerque, NM, 2016.

[22] K. Zeng, Optimization of support structures for selective laser melting, University of Louisville, Kentucky (USA), 2015.
[23] E. Strumza, S. Hayun, S. Barzilai, Y. Finkelstein, R. Ben David, O. Yeheskel, In situ detection of thermally induced porosity in additively manufactured and sintered objects, J. Mater. Sci. 54 (2019) 8665–8674. https://doi.org/10.1007/s10853-019-03452-5.
[24] B. Buchmayr, G. Panzl, A. Walzl, C. Wallis, Laser Powder Bed Fusion – Materials Issues and Optimized Processing Parameters for Tool steels, AlSiMg- and CuCrZr-Alloys, Adv. Eng. Mater. 19 (2017) 1600667. https://doi.org/10.1002/adem.201600667.

Appendix: Model building and first results (global presentation)

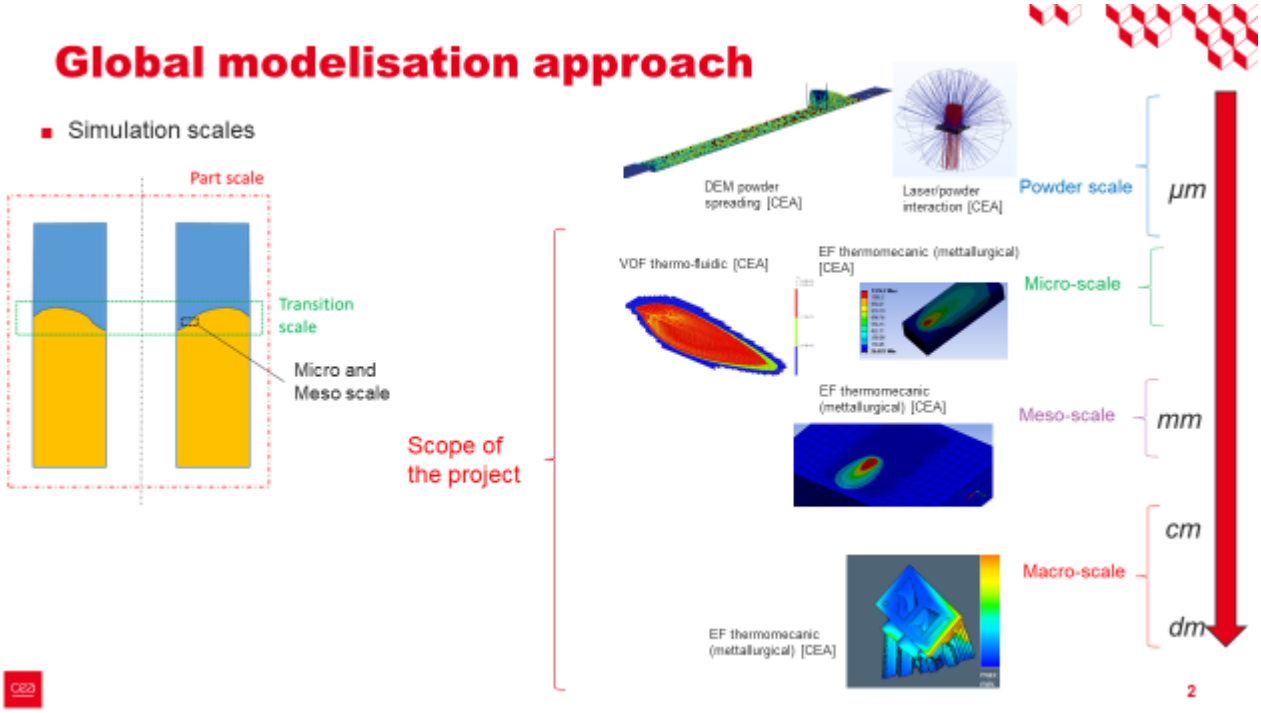

Micro and Meso thermal model for L-PBF bimaterial configuration

27-11-2023

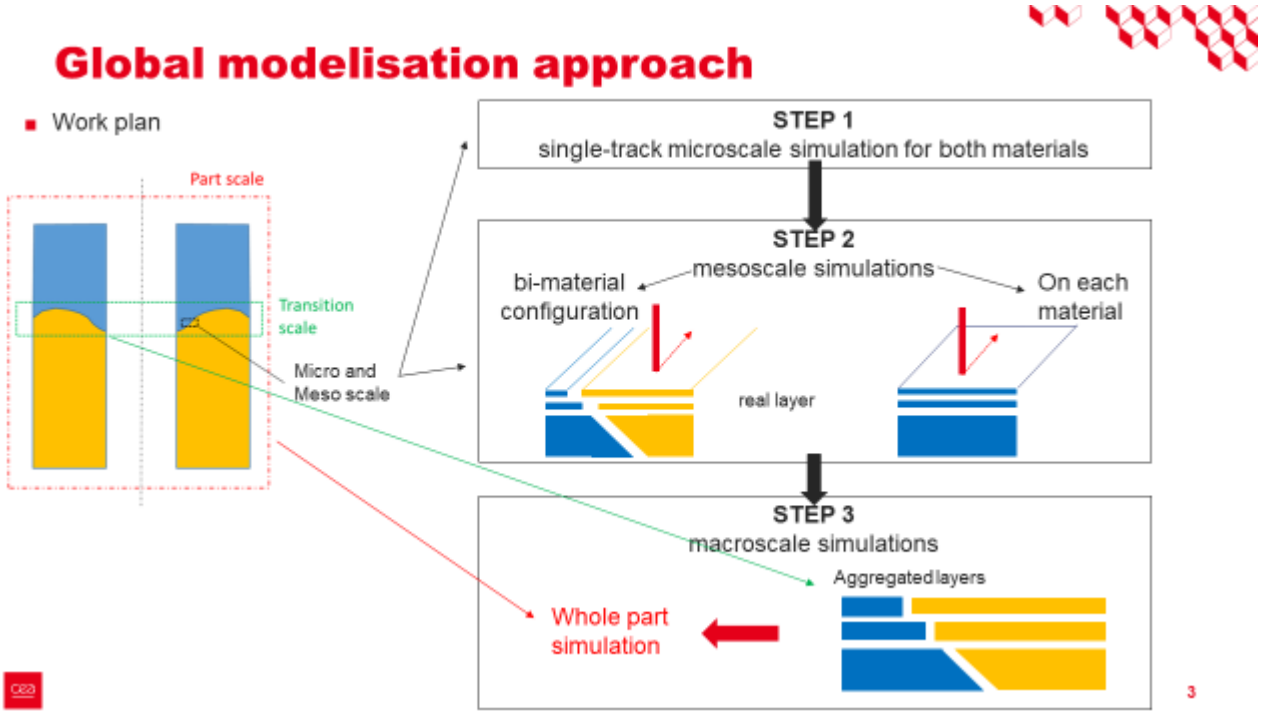
Global modelisation approach
Work plan
Part scale
Transition scale
Micro and Meso scale
STEP 1
single-track microscale simulation for both materials
STEP 2
mesoscale simulations
bi-material configuration
On each material
real layer
STEP 3
macroscale simulations
Aggregated layers
Whole part simulation
3

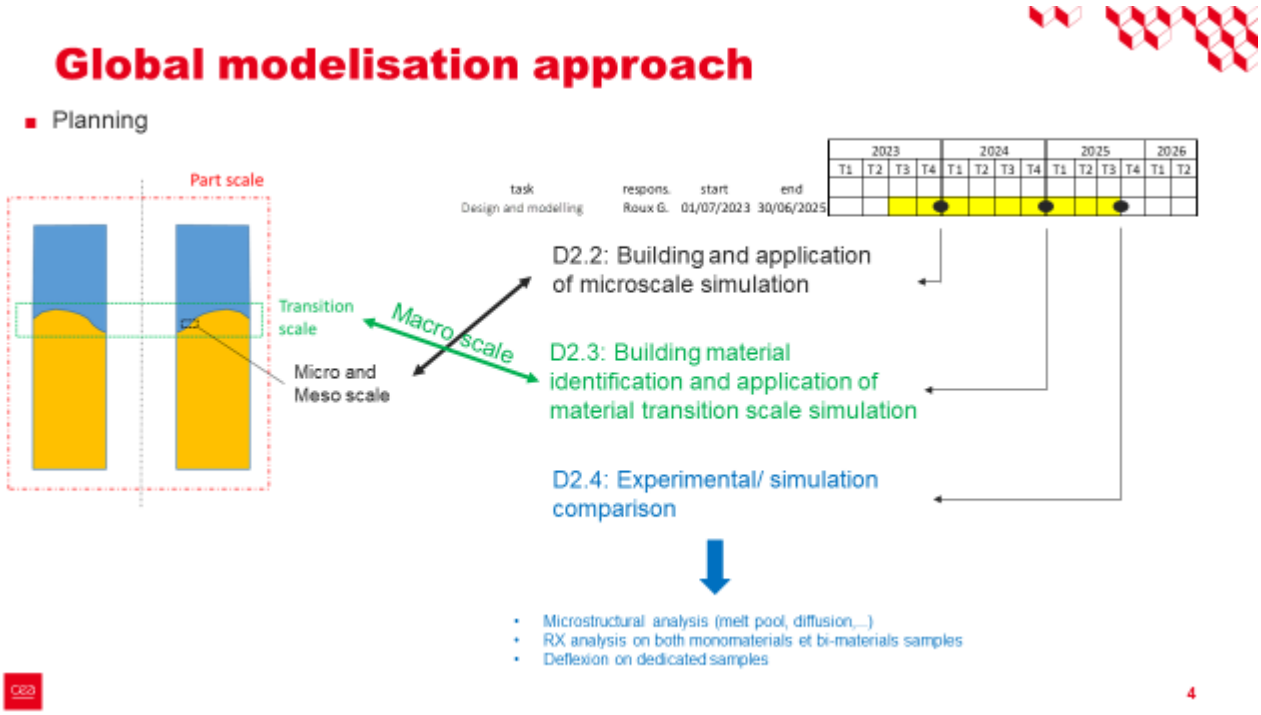
Global modelisation approach
Planning
Part scale
Transition scale
Micro and Meso scale
Macro scale
task
respons.
start
end
Design and modelling
Roux G.
01/07/2023
30/06/2025
2023
2024
2025
2026
T1 T2 T3 T4 T1 T2 T3 T4 T1 T2 T3 T4 T1 T2
D2.2: Building and application of microscale simulation
D2.3: Building material identification and application of material transition scale simulation
D2.4: Experimental/ simulation comparison
Microstructural analysis (melt pool, diffusion,...)
RX analysis on both monomaterials et bi-materials samples
Deflexion on dedicated samples
4

Models description: Thermal

- Physics

$$\rho C_p \frac{\partial T}{\partial t} = \frac{\partial}{\partial x}\left(k\frac{\partial T}{\partial x}\right) + \frac{\partial}{\partial y}\left(k\frac{\partial T}{\partial y}+\right)\frac{\partial}{\partial z}\left(k\frac{\partial T}{\partial z}\right) + Q$$ Heat conduction equation

Q is volumetric heat: volumetric laser source and/or latent heat effects

- Geometric configuration

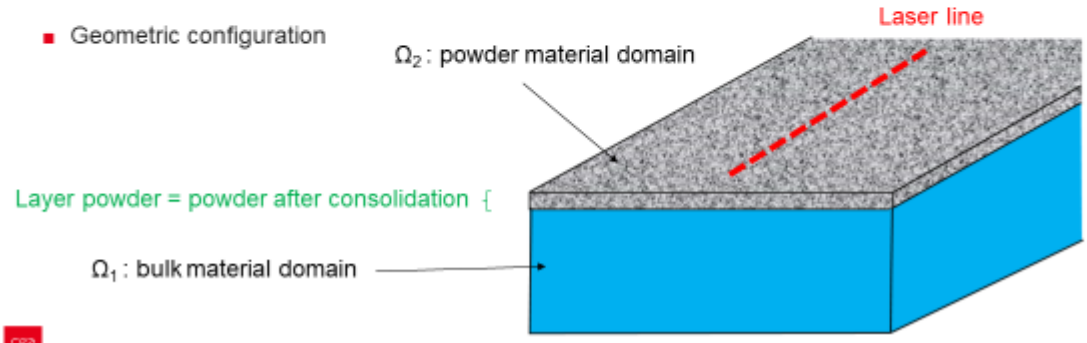

5

Models description: Thermal

- Boudaries conditions
  - Laser heat source

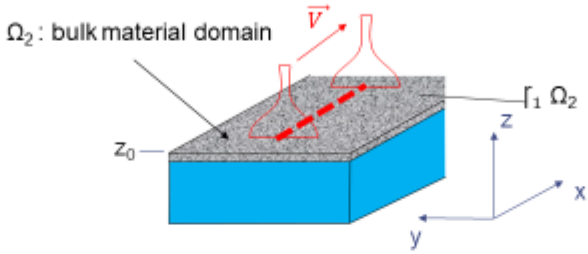

→ surfacic Gaussian heat source $Q(x,y) = \frac{2\lambda P_L}{\pi r_L^2} exp\left(\frac{-2[(x-x_0)^2+(y-y_0)^2]}{r_L^2}\right)$ For z∈ Γ_1

used for our simulations

→ volumic Gaussian heat source with Beer-Lambert absorption law

[Makoana et al., 2018] $Q(x,y) = \frac{2\lambda P_L \beta}{\pi r_L^2} exp\left(\frac{-2[(x-x_0)^2+(y-y_0)^2]}{r_L^2}\right) exp(-\beta|z-z_0|)$ For z∈ Ω

$\beta = \frac{1}{L_{ep}}$ as few laser penetration through bulk material

6

Models description: Thermal

With:

x_0, y_0	Position of laser on the path → lasing strategy and laser velocity V_L
z_0	Upper heigh of lased layer
r_L	Beam radius (80µm for SLM125HL equipment)
S_L	Penetration parameter
λ	Laser power absorptivity

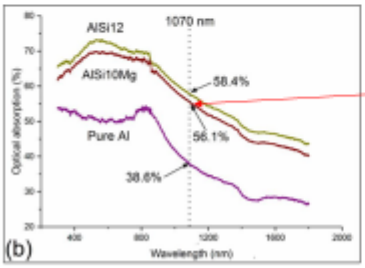

CuCrZr: 0.42

AlSi10Mg: 0.56

[Tissot, 2019]

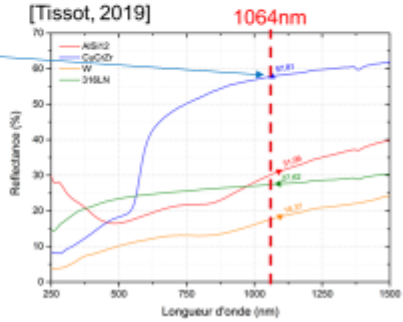

[Ghasemi *et al.*, 2021]

Models description: Thermal

- Boudaries conditions
  - Upper heat losses

→ radiation

$-k\nabla T.\vec{n} = q_{ray}(x,y) = \sigma\xi(T^4 - T_0^4)$ for z∈ Γ_1

T_0	Ambiant temperature
σ	Stephan-Boltzmann constant
ξ	emissivity

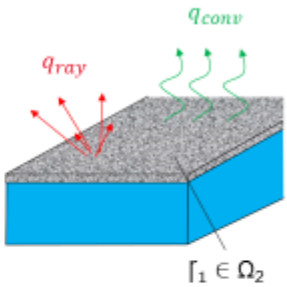

→ forced convection (gas flow inside chamber)

$-k\nabla T.\vec{n} = q_{conv}(x,y) = h(T - T_0)$ | h Forced convection coeficient

To limit conputation time, combinated equivalent convection losses

$h_{eq} = 24.1E^{-4}\xi(T - 273)^{1.61}$ | with $\xi = 0.9$

[Goldak *et al.*, 1984]

8

Models description: Thermal

- Boudaries conditions
  - Fixed temperature at bottom of studied part

$T = T_B$ for Γ_2

→ bottom temperature depends on process parameters, plate configuration and **wich layer considered**

→ temperature fixed at T_B=80°C (first layers)

→ bottom temperature can be simulated using aggregated macroscopic approach

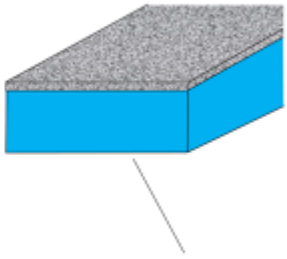

$\Gamma_2 \in \Omega 1$

9

Models description: Thermal

- Powder zone properties

→ Packed bed powder conductivity can be approximated by:

$$k_P = \frac{\frac{\rho}{\rho_S} k_S}{1 + \Phi \frac{k_S}{k_{gas}}}$$

$$\Phi = 0.02 E^{(2(0.7-\rho_b))}$$

Very low conductivity

k_S	Bulk conductivity
k_{gas}	Surrounded gas conductivity conductivity
$\frac{\rho}{\rho_S}$	Packed bed relative density

[Bugeda et al., 1999]

→ To avoid numerical problem, we impose $k_P = 0.1 k_b$

→ As powder zone is considered geometrically as consolidated

$\rho_P = \rho_b$

$C_P = C_b$

10

Models description: Thermal

- Liquid/Solid transformation

→ Phase change is take into account by parameters dépendance in temperature (no metallurgical change in our case)

→ conductivity:

$$k_L = k_S \quad \text{for} \quad T < T_m$$

$$k_L = 2.5k_S \quad T < T_m$$

[Ren et al., 2019]

→ heat capacity:

$$C_L = C_S \quad \text{for} \quad T < T_m - 0.5\Delta T_m \quad \text{or} \quad T > T_m - 0.5\Delta T_m$$

$$C_L = C_S + \frac{L}{\Delta T_m} \quad \text{for} \quad T_m - 0.5\Delta T_m < T < T_m + 0.5\Delta T_m$$

[Promoppatum et al., 2017]

→ Bad.....too much step size dependant. I programed phase change and so heat generation with phase change within convergence iterations

[Tang, 2017], $AlSi_{10}Mg$

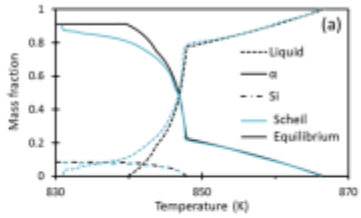

[Wisniewski, 2017], CuCrZr

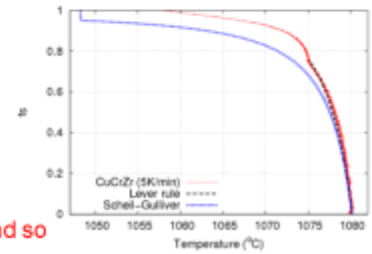

11

Materials thermal properties

[Stefan et al., 2016]
SLMed AlSi10Mg0.6

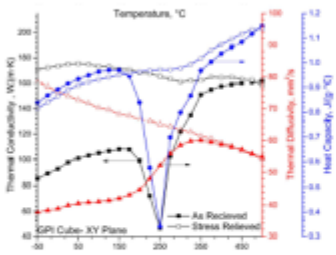

Precipitation zone

[Zeng et al., 2021]
SLMed CuCrZr

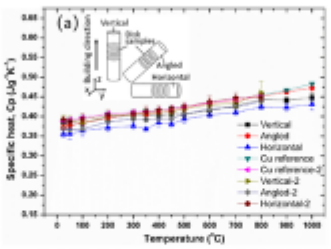

First thermal cycle

second thermal cycle

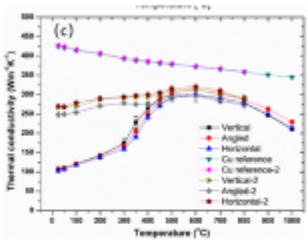

Precipitation zone

→ As built properties are considered

→ precipitation won't occurs on top layers, so evolutions in this zone are excluded

→ First cycle properties are considered (as built state)

12

Materials thermal properties

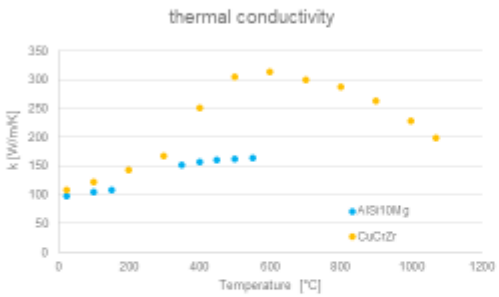

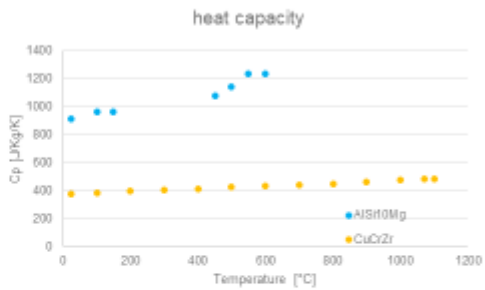

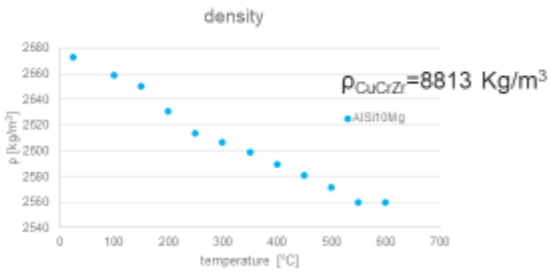

13

Models description: Mechanical

- Physics

$\nabla.\{\sigma\} + \rho\vec{b}$ Quasi-static stress equilibrium

$\{\sigma\}$ stress tensor

$\vec{b}$ Internal body force per unit volume

- Geometric configuration

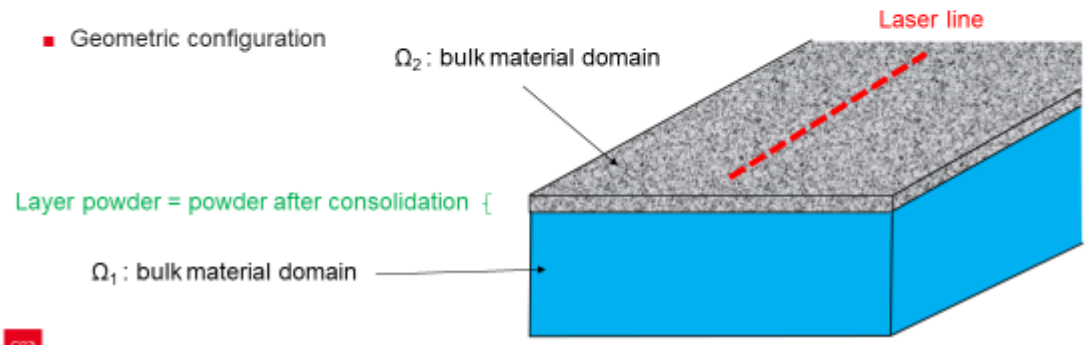

14

Models description: Mechanical

- Material behavior

For bulk material domain Ω_1: $\{\sigma\} = [C]\{\varepsilon^e\}$

$[C]$ 6x6 elasticity matrix

$\{\varepsilon^e\}$ elastic strain tensor

We suppose isotropic mechanical behavior: $\{\sigma\} = \frac{E}{1+\nu}\left(\{\varepsilon^e\} + \frac{\nu}{1-2\nu} Tr\{\varepsilon^e\}\{I\}\right)$

E Young modulus

ν Poisson ratio

Strain partition is defined by: $\{\varepsilon^t\} = \{\varepsilon^e\} + \{\varepsilon^p\} + \{\varepsilon^{th}\}$

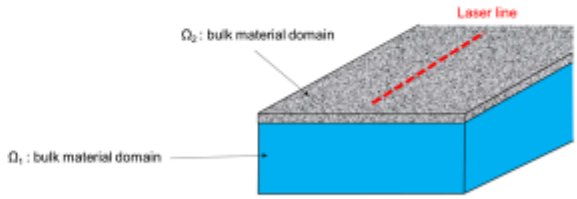

$\{\varepsilon^t\}$ total strain tensor

$\{\varepsilon^t\}$ plastic strain tensor

$\{\varepsilon^{th}\}$ dilatation strain tensor $\{\varepsilon^{th}\} = \alpha[T - T_{ref}]\{I\}$

α Poisson coeficient

T_{ref} reference temperature for $\{\varepsilon^{th}\} = \{0\}$

Models description: Mechanical

We suppose isotropic purely J_2 plasticity: $f(\{\sigma\}) = \sqrt{\frac{\{S\}:\{S\}}{2}} - \sigma_y$

$\{S\} = \{\sigma\} - \frac{1}{3}Tr\{\sigma\}$

σ_y Yield stress

For powder material domain Ω_2: $\{\sigma\} = [C][\{\varepsilon^t\} - \underbrace{\{\epsilon^{th}\}}_{\text{Same as bulk material}}]$ Purely elastic material

Powder has no rigidity → $E_{powder}=E_{bulk}\cdot 10^{-7}$

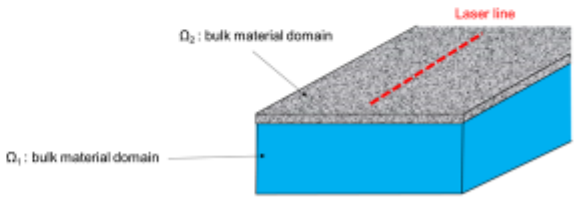

Mechanical properties of AlSI10Mg

- Thermo-elastic properties

[Strumza, 2019]

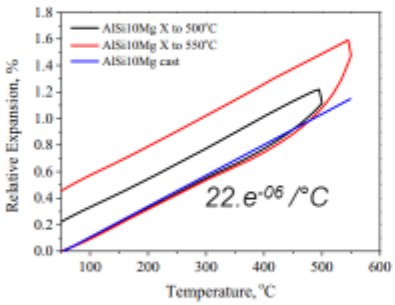

[Soylemez, 2019]

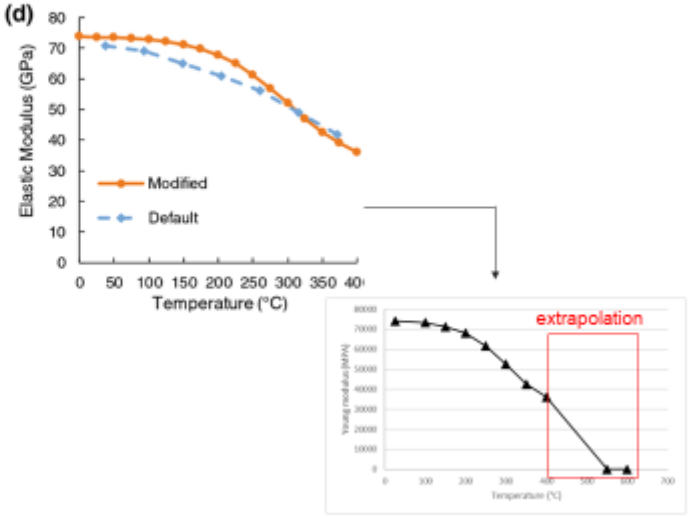

17

Mechanical properties of AlSI10Mg

- Plasticity

[Uzan, 2018], L-PBF

Table 1. Mechanical properties of AM-SLM AlSi10Mg specimens at various temperatures.

Test temperature, °C	Elastic modulus (E), GPa	Yield stress (YS), MPa	Ultimate tensile stress (UTS), MPa	Elongation at fracture (e), %	Reduction of area, %
25	77.6	204	358	7.2	8.7
50	75.5	198	341	8.5	9.2
100	72.8	193	286	10.0	11.1
150	*	182	241	14.7	15.8
200	*	158	189	16.4	18.7
250	*	132	149	38.9	58.3
300	*	70	73	48.4	67.4
350	*	30	33	53.8	81.9
400	*	12	14	57.4	98.0

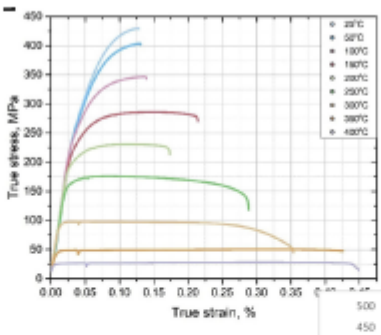

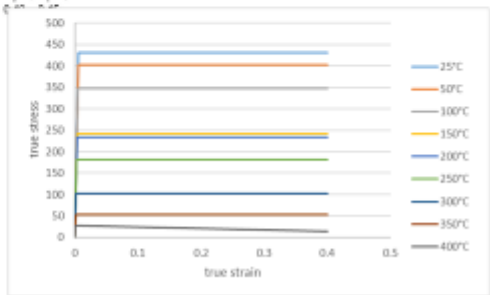

→ In a first step, we choose a perfect plasticity with ultimate true stress limit =maximisation of residual stresses

18

Mechanical properties of CucrZr

- Thermo-elastic properties

[Ferraiuolo, 2023]

Temperature [K]	Mass Density [kg/m^3]	Thermal Conductivity [W/mK]	Specific Heat [J/kgK]	Thermal Expansion Coefficient [1/K]
300	8933	320	390	15.7×10^{-6}
600	8933	290	390	17.9×10^{-6}
900	8933	255	400	18.7×10^{-6}

[Zhang, 2019]

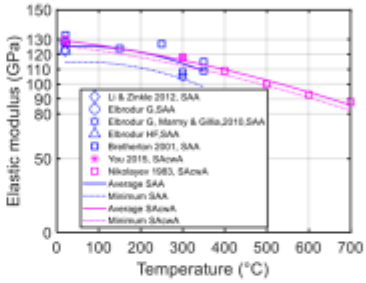

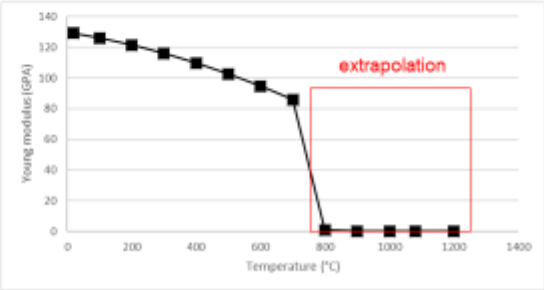

19

Mechanical properties of CuCrZr

- Plasticity

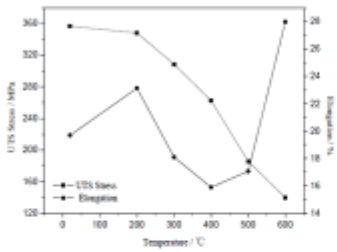

[Zhang et al., *2015]*

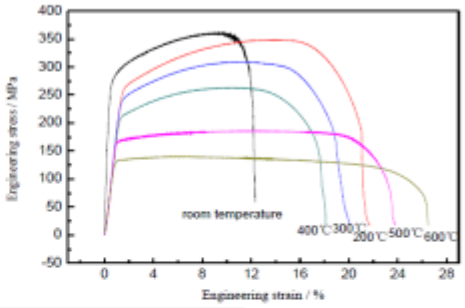

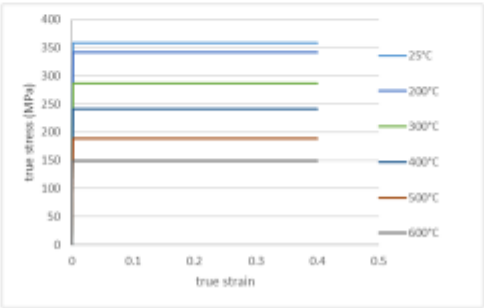

20

Process parameters

	$AlSi_{10}Mg$ [Rausch et al., 2017]	CuCrZr [Buchmayr et al., 2017]
Power [W]	350	370
speed [mm/s]	1650	300
hatch distance [mm]	0.13	0.11
layer thickness [µm]	30	20

For both materials we will consider:

- 30µm layer thickness
- 80µm laser diameter

All these parameters will be updated after material process consolidation

SLM 125HL

21

Geometric configuration for monotrack

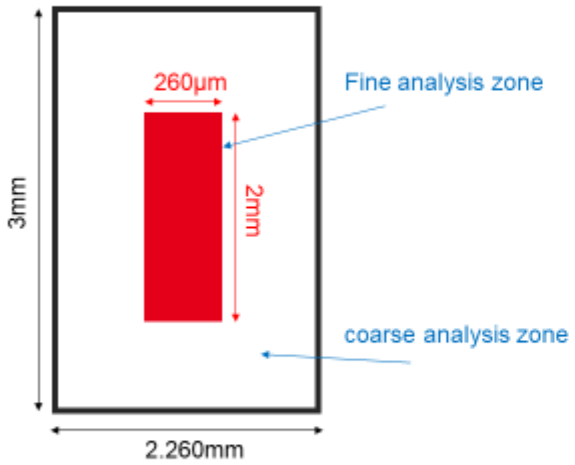

View of the mesh

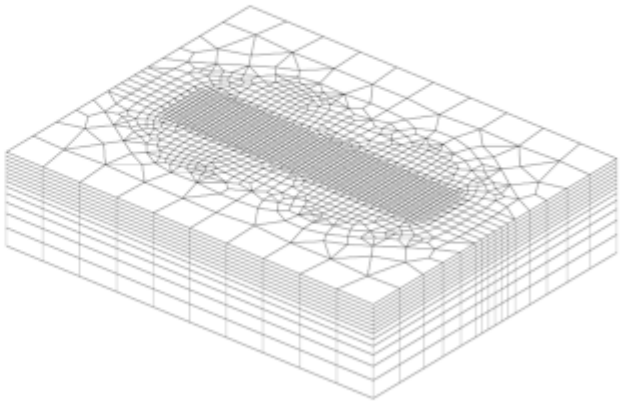

Solver configuration: no latent heat effect

22

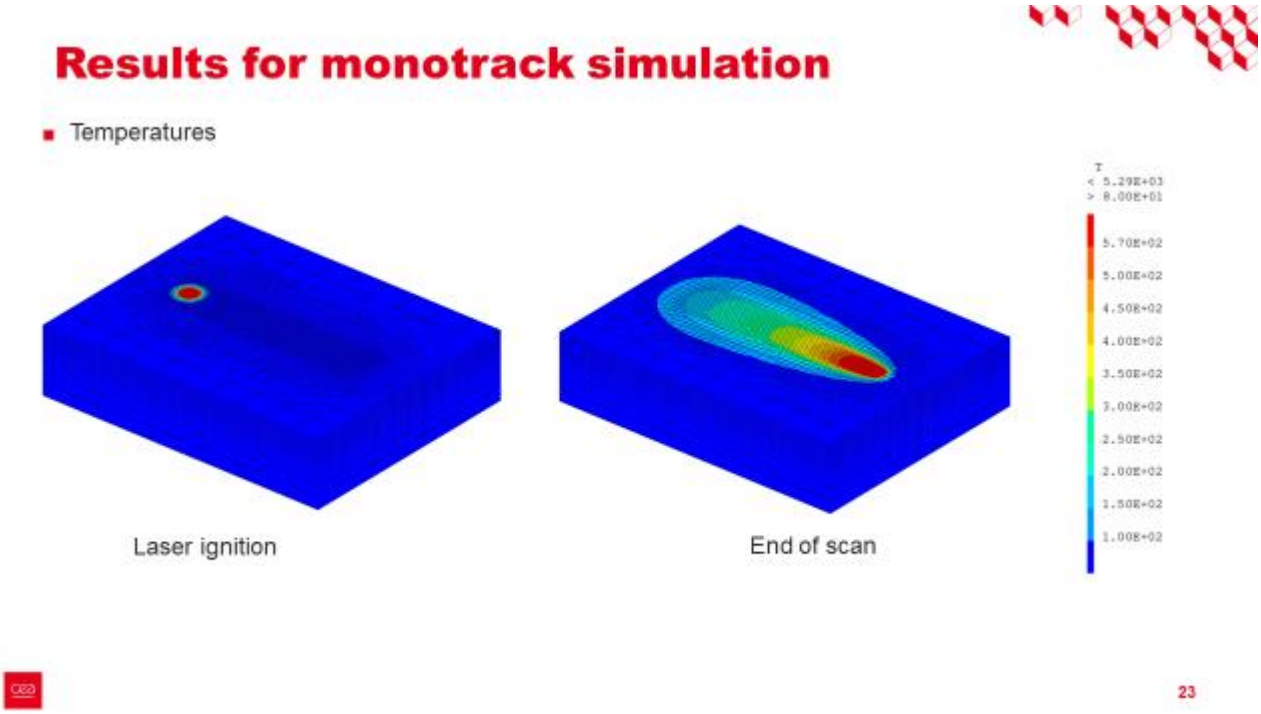
Results for monotrack simulation
Temperatures
Laser ignition
End of scan
23

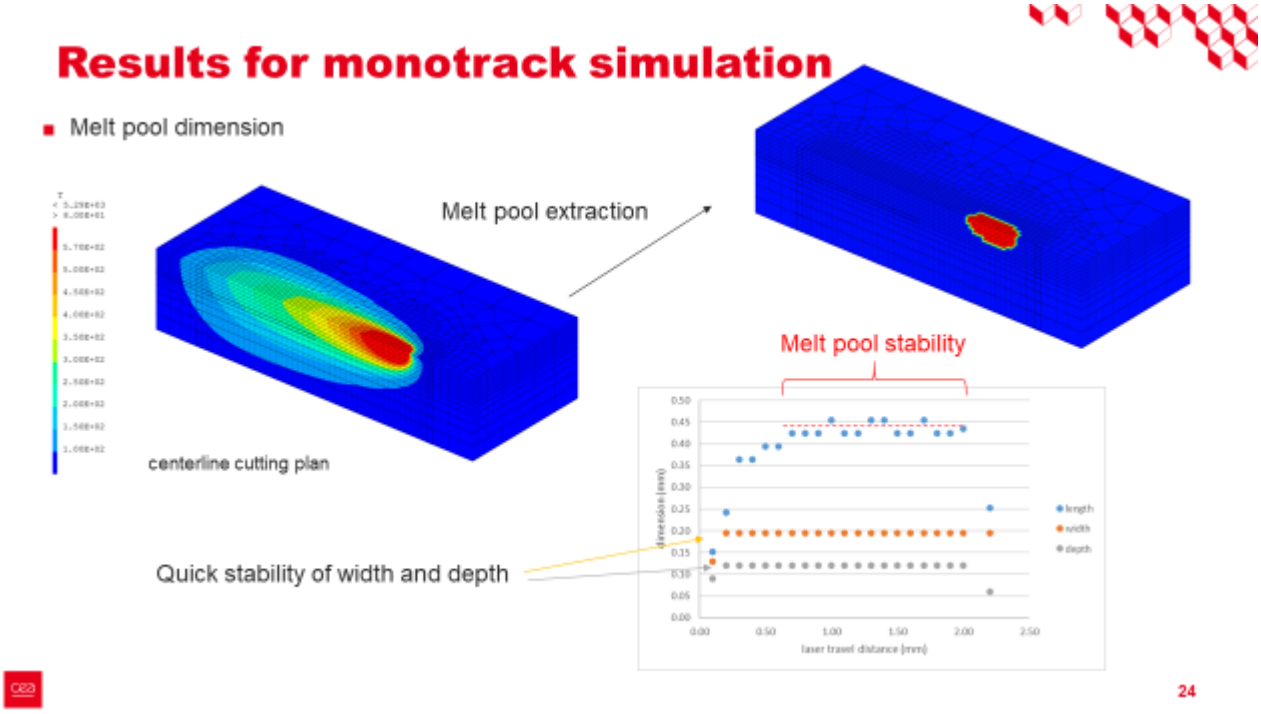
Results for monotrack simulation
Melt pool dimension
Melt pool extraction
centerline cutting plan
Melt pool stability
Quick stability of width and depth
24

Results for monotrack simulation

- Comparaison with analytic model

Our work

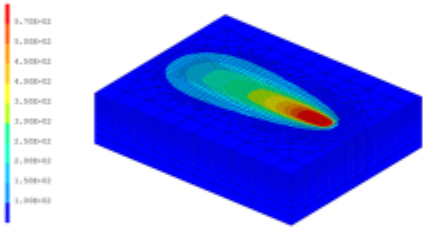

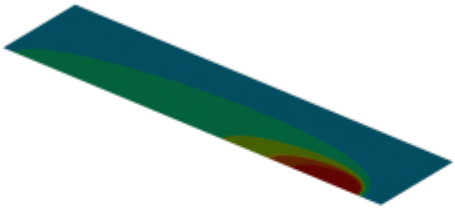

Rosenthal solution [Rosenthal, 1941]:

$$T = T_0 + \frac{\lambda P}{2\pi k r} e^{\left[-\frac{V(r+\xi)}{2\alpha}\right]}$$

x, y, z distance from source

k thermal conductivity

α thermal diffusivity

k radial distance from source

$\xi = x - V.t$

25

Results for monotrack simulation

- Comparaison with analytic model

	Rosenthal solution	our work
length [µm]	537	439.5
width [µm]	272	195
depth [µm]	136	120

Rosenthal solution overestimate melt pool dimensions

Known from litterature

[Promoppatum, 2017], IN718

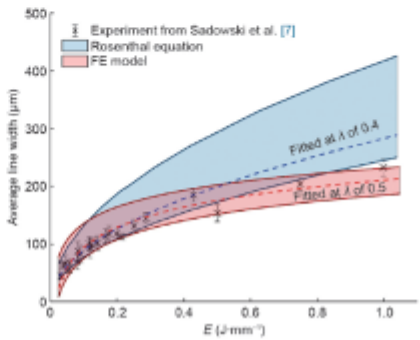

26

Results for monotrack simulation

- Influence on model complexity on melt pool dimension and computation time

simul	NL thermal properties	liquid conductivity	powder/bulk phase change	latent heat	time [ms]	time (min)	factor	melt pool dimension length [ym]	width [ym]	depth [ym]
1					605171	10	1.00	530	195	120
2	x				1780593	30	2.94	485	195	120
3	x	x			5317359	89	8.79	394	260	120
4	x	x	x		5561562	93	9.19	432	195	120
5	x		x		2362374	39.3729	3.90	545	195	120
6				x	2453484	41	4.05	909	195	90
7	x	x		x	16134422	269	26.66	667	195	90

Sim 5

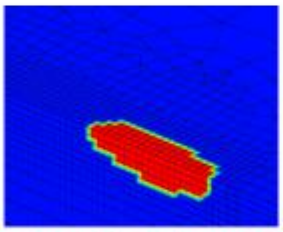

Sim 7

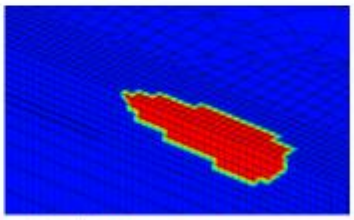

Transverse section of the melt pool is the most important for residual stresses generation → layent heat play a major role in transverse melt pool dimension

27

Results for monotrack simulation

- Melted powder

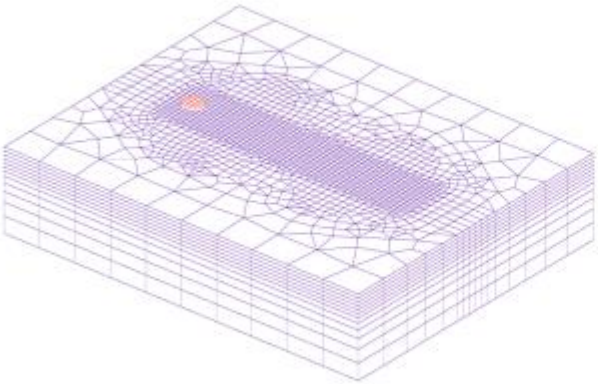

Laser ignition

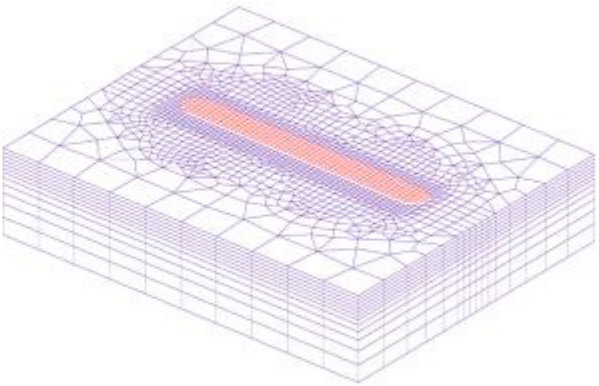

End of scan

28

Results for monotrack simulation

- Stress field during lasing

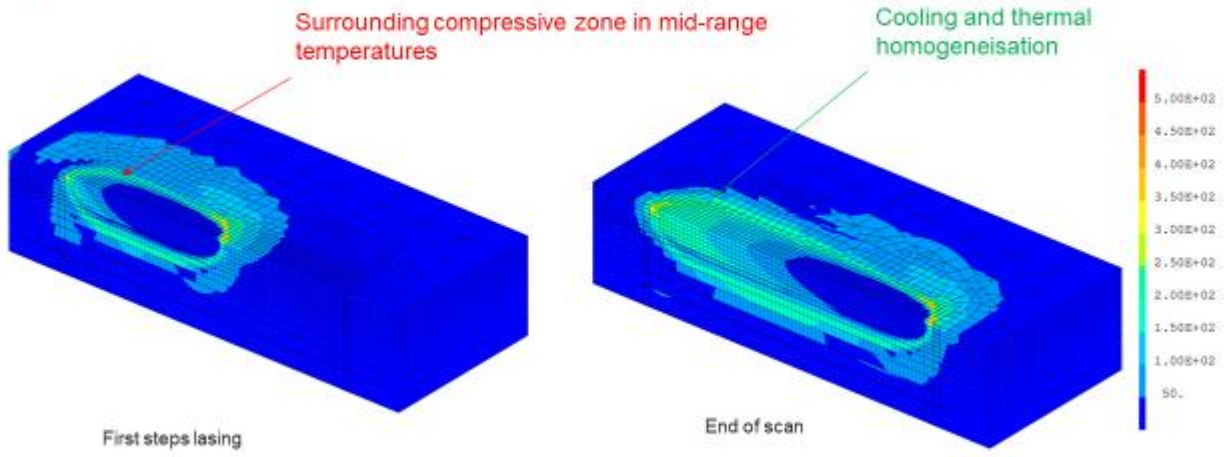

29

Results for monotrack simulation

- Residual stresses

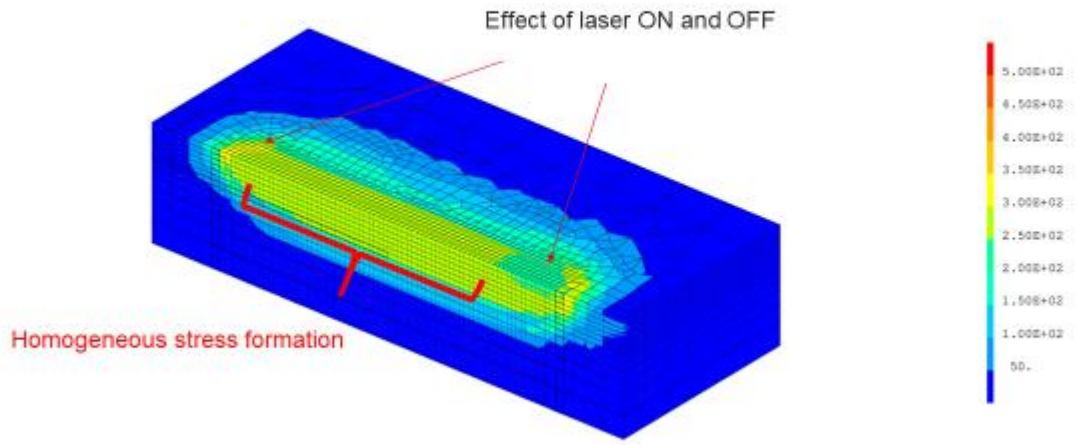

30

Results for monotrack simulation

- Residual stresses σ_{xx}

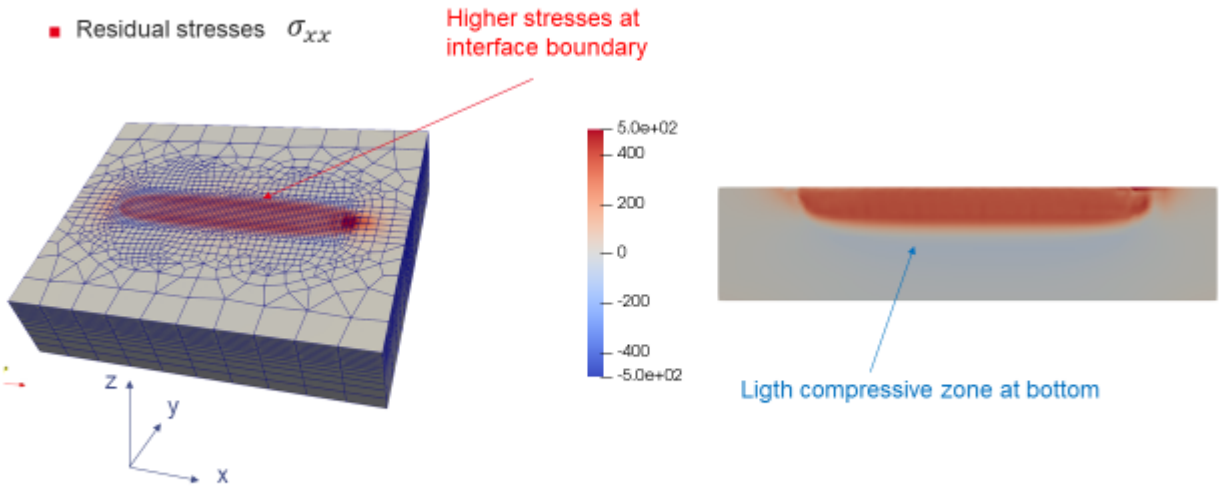

Traction stresses in lasing direction, mainly localized in melt pool and near melt pool zones

31

Results for monotrack simulation

- Residual stresses σ_{yy}

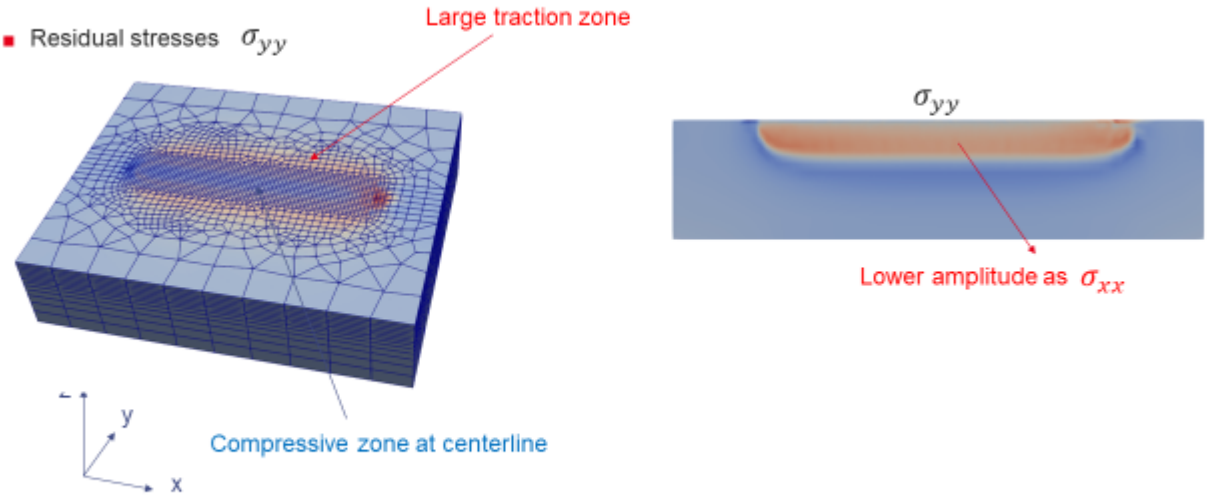

Large tensile stress region in transverse direction, with less amplitude than in lasing direction

32

Results for monotrack simulation

- Residual stresses σ_{zz}

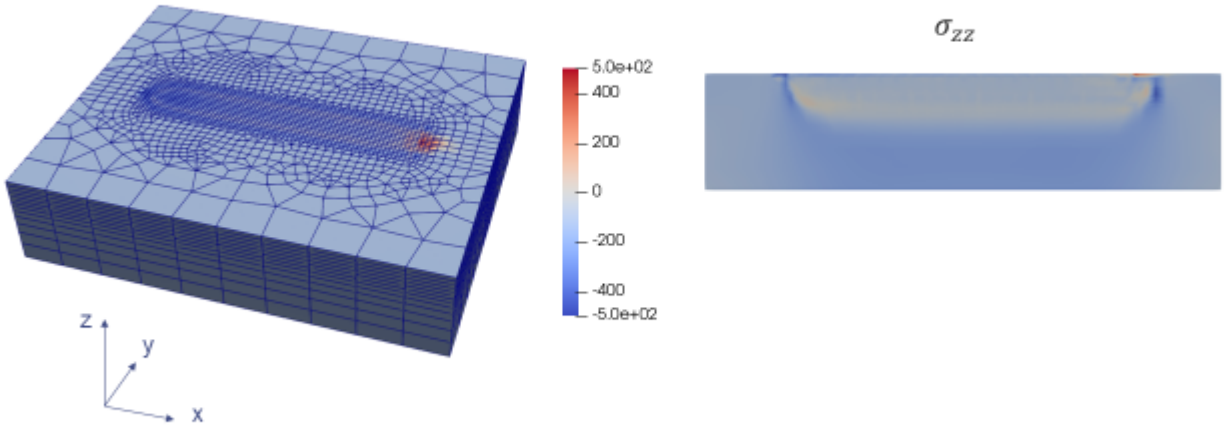

Low stresses in vertical direction, mainly compressive ones

33

Geometric configuration for mesoscopic simulation

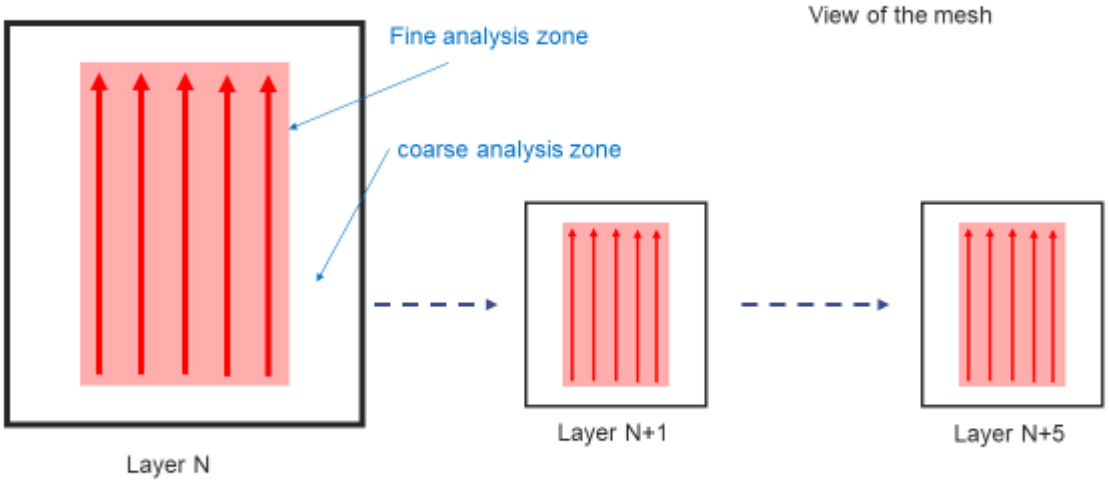

Solver configuration: linear thermal model

Lasing strategy can be changed

34

Geometric configuration for mesoscopic simulation

View of the mesh:

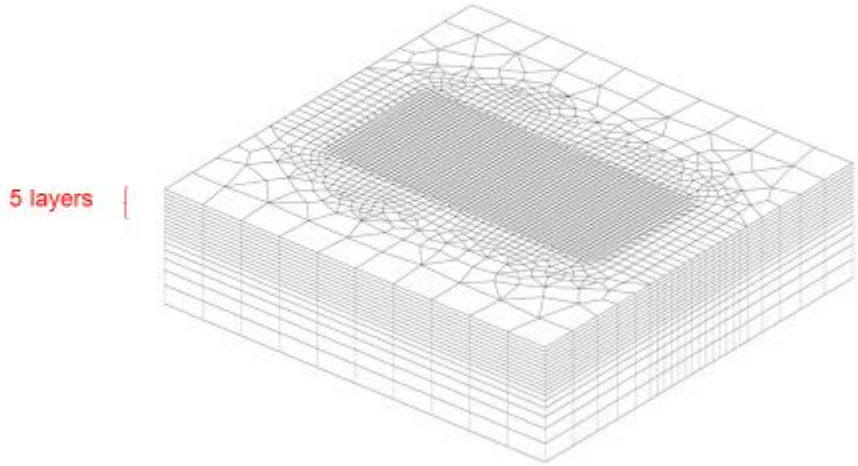

35

Geometric configuration for mesoscopic simulation

→ supposed test sample

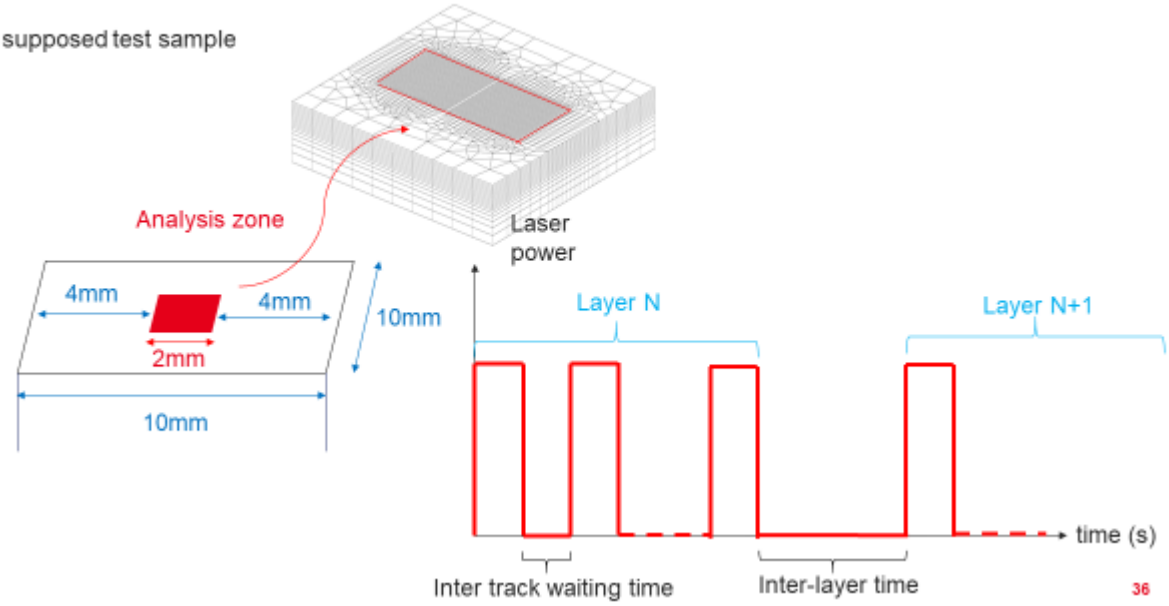

36

Results for mesoscopic simulation

- Temperatures

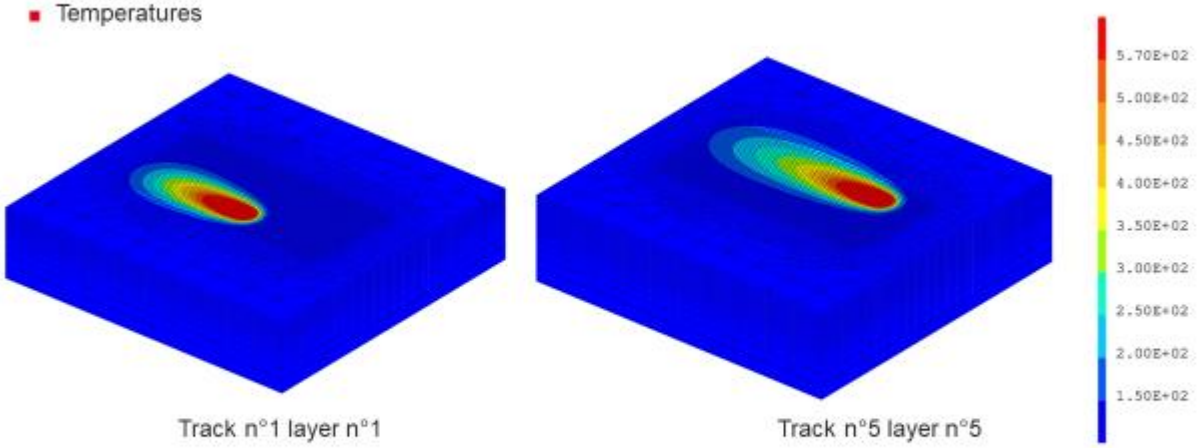

37

Results for mesoscopic simulation

- Temperatures evolution with contiguous tracks

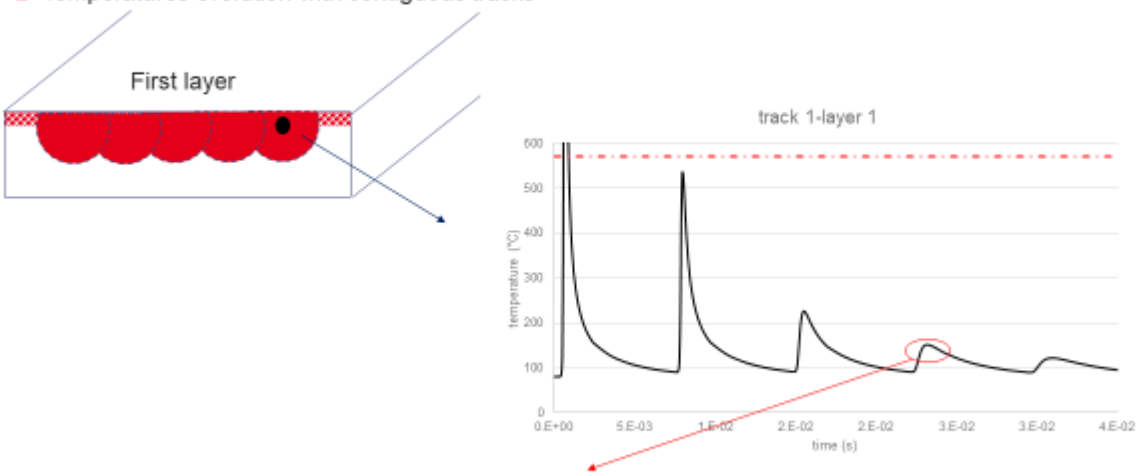

One track is no more thermally (and mechanically ?) affected (+100°C) after 3 contiguous tracks

38

Results for mesoscopic simulation

- Temperatures evolution with contiguous tracks

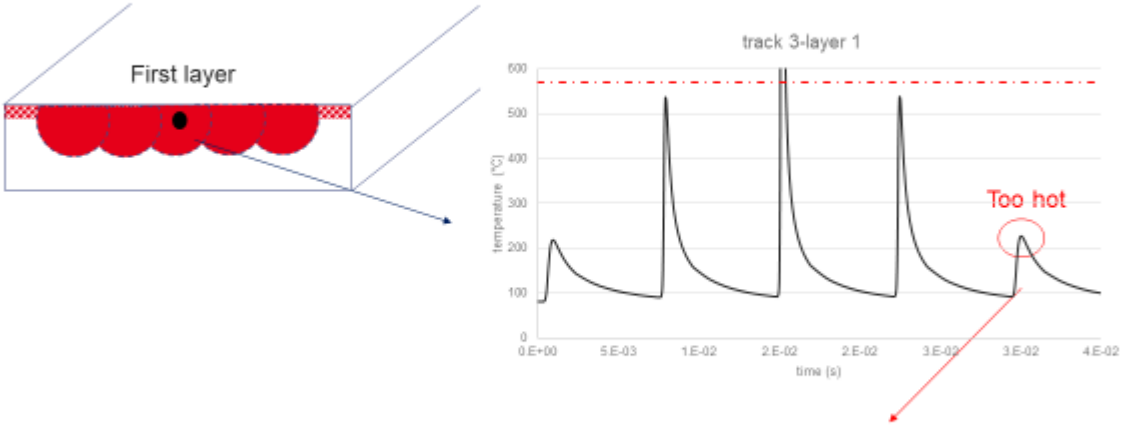

- If we want to reach representative thermal evolution, we need to have at least 2 more tracks → 5+2=7 tracks
- If we want at least 3 representative tracks → 7+2=**9 tracks**

39

Results for mesoscopic simulation

- Temperatures evolution with layers

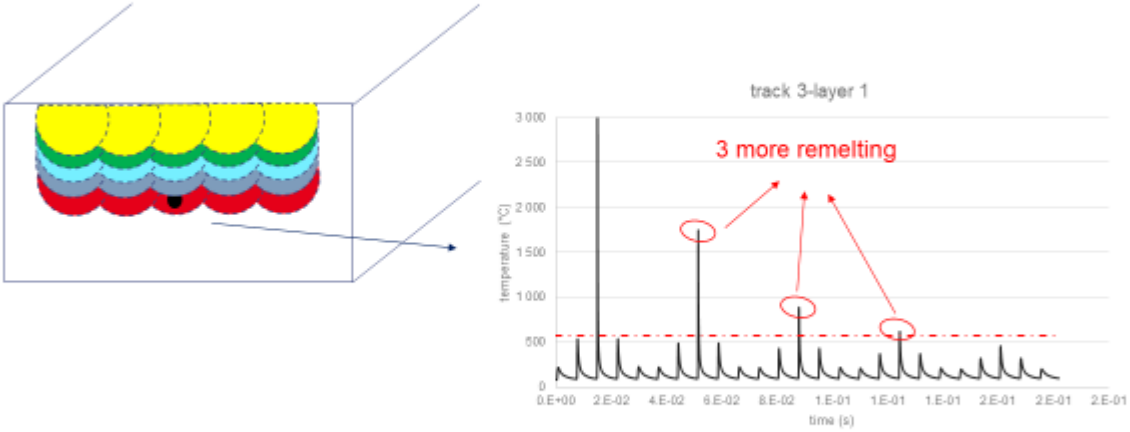

A least 10 layers are necessary to acheive representative thermal evolution

40

Results for mesoscopic simulation

- V.M. Stress field after first layer

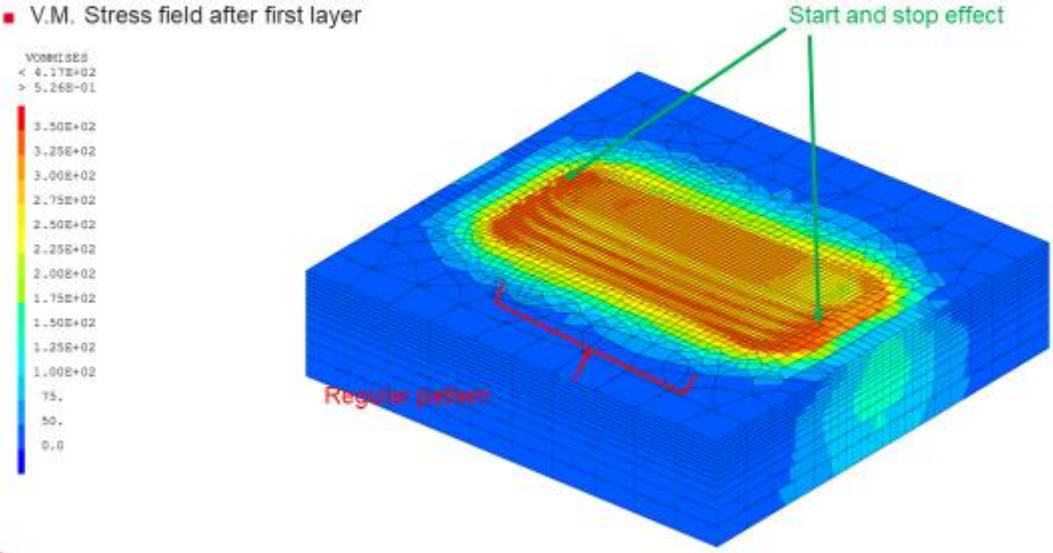

41

Results for mesoscopic simulation

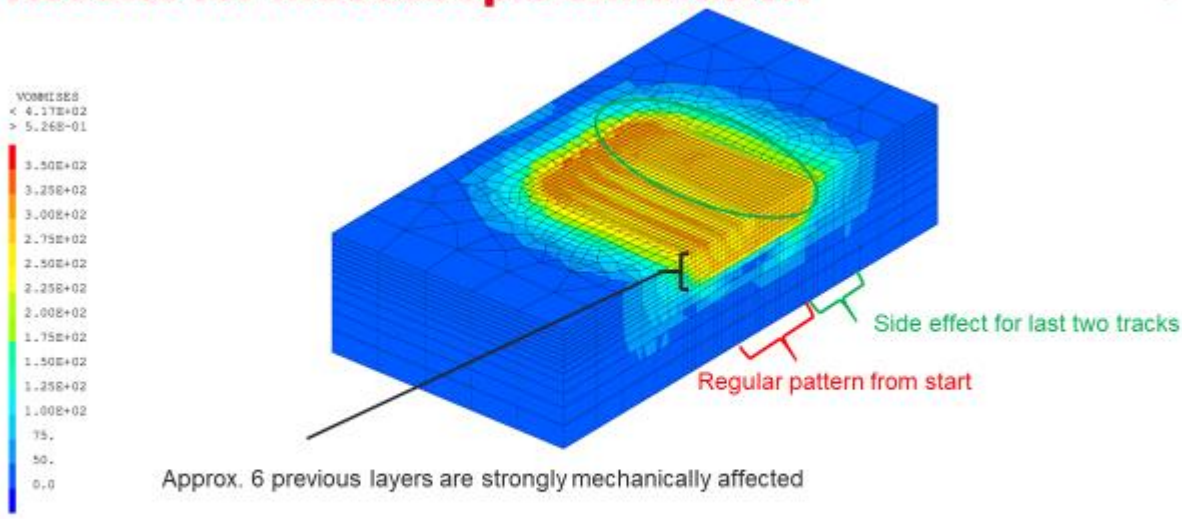

Approx. 6 previous layers are strongly mechanically affected

→ It is not necessarry to have a lot of tracks per layer

42

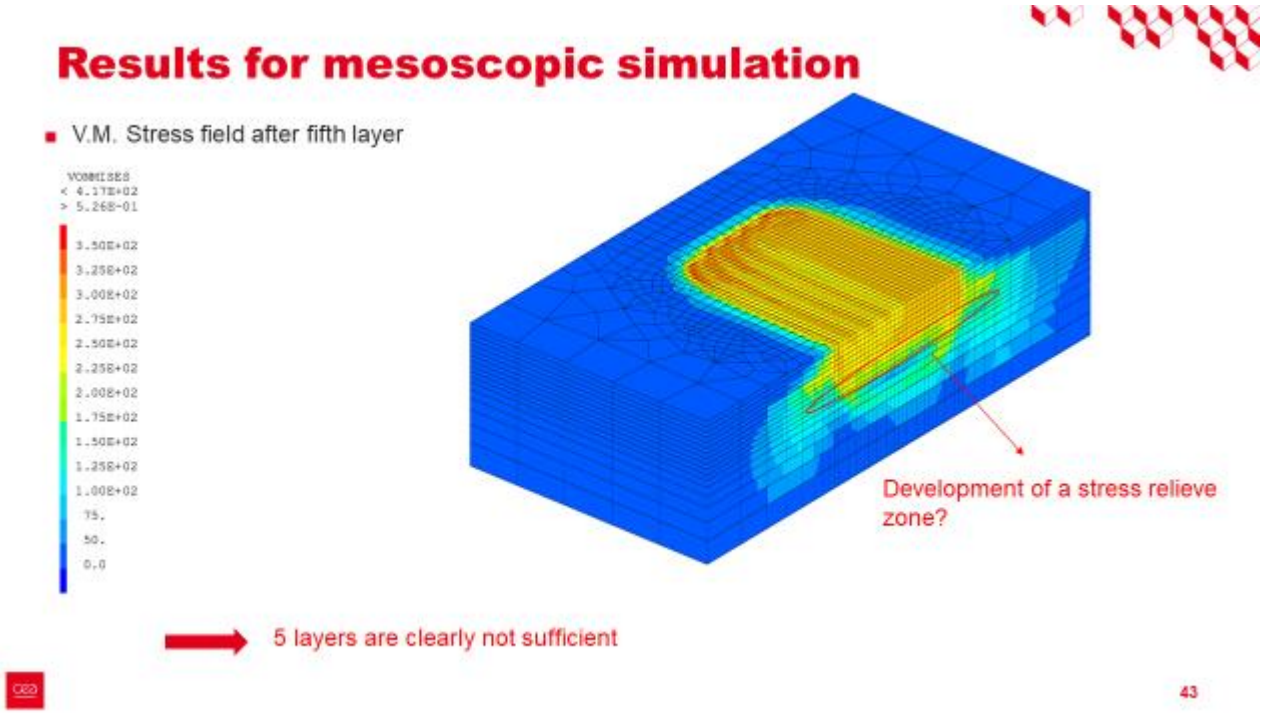
Results for mesoscopic simulation
V.M. Stress field after fifth layer
VONMISES
< 4.17E+02
> 5.26E-01
3.50E+02
3.25E+02
3.00E+02
2.75E+02
2.50E+02
2.25E+02
2.00E+02
1.75E+02
1.50E+02
1.25E+02
1.00E+02
75.
50.
0.0
Development of a stress relieve zone?
5 layers are clearly not sufficient
43

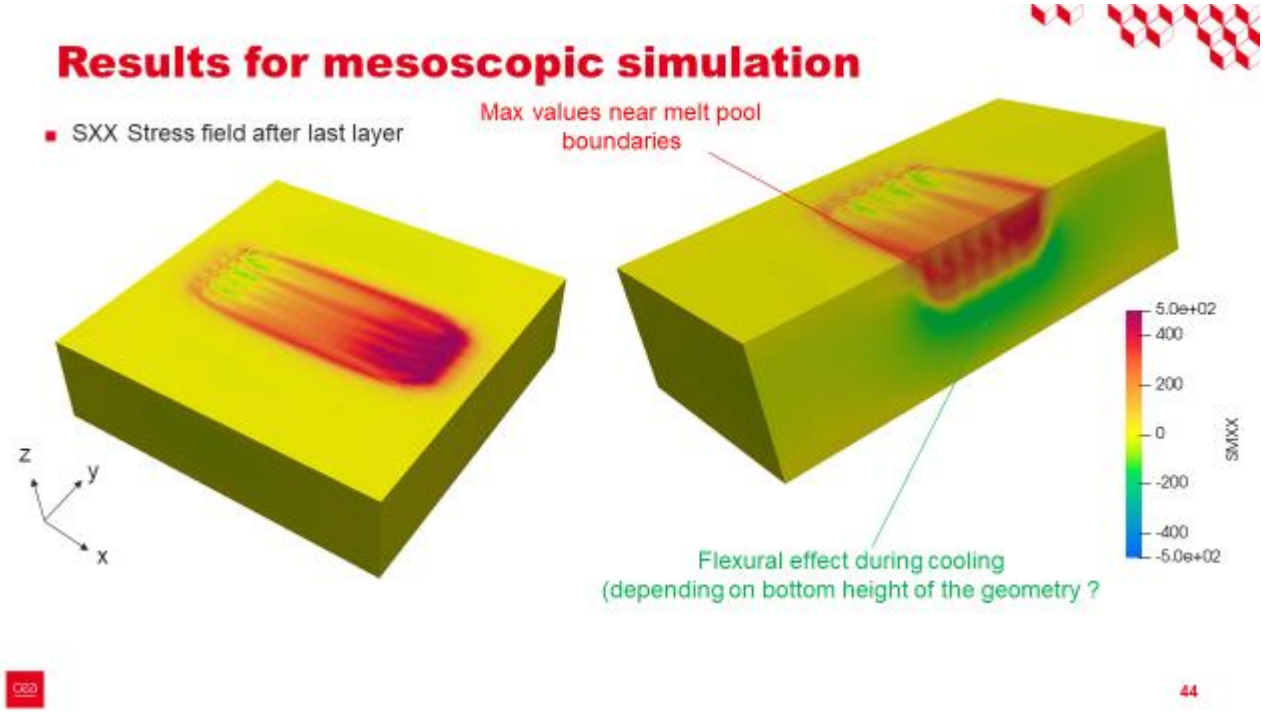
Results for mesoscopic simulation
SXX Stress field after last layer
Max values near melt pool boundaries
z
y
x
5.0e+02
400
200
0
-200
-400
-5.0e+02
SMXX
Flexural effect during cooling
(depending on bottom height of the geometry ?
44

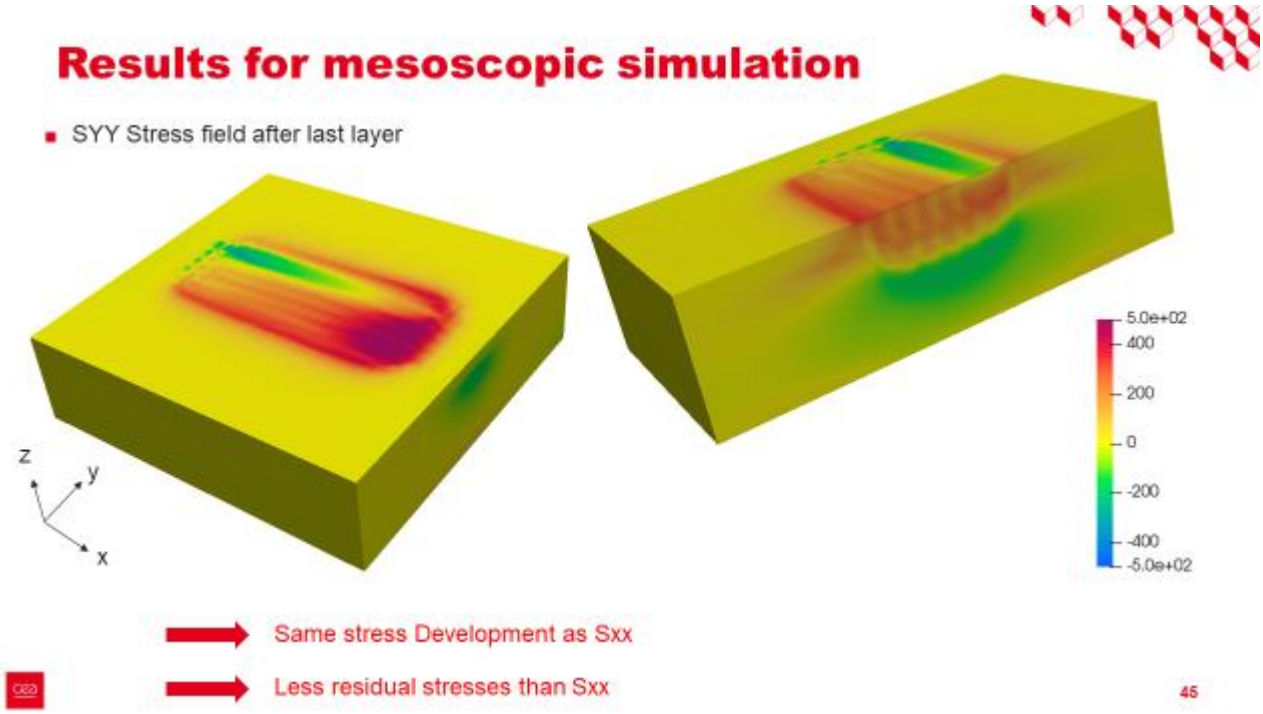
Results for mesoscopic simulation
SYY Stress field after last layer
5.0e+02
400
200
0
-200
-400
-5.0e+02
z
y
x
Same stress Development as Sxx
Less residual stresses than Sxx
45

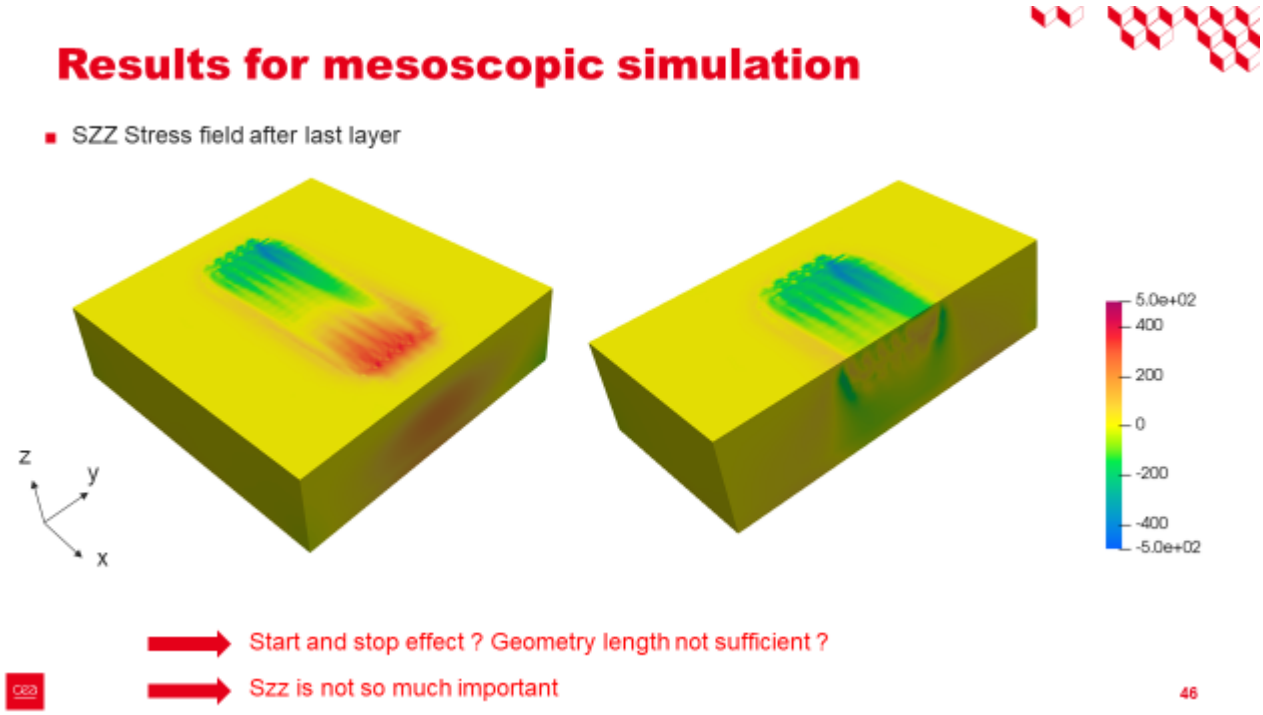
Results for mesoscopic simulation
SZZ Stress field after last layer
5.0e+02
400
200
0
-200
-400
-5.0e+02
z
y
x
Start and stop effect ? Geometry length not sufficient ?
Szz is not so much important
46

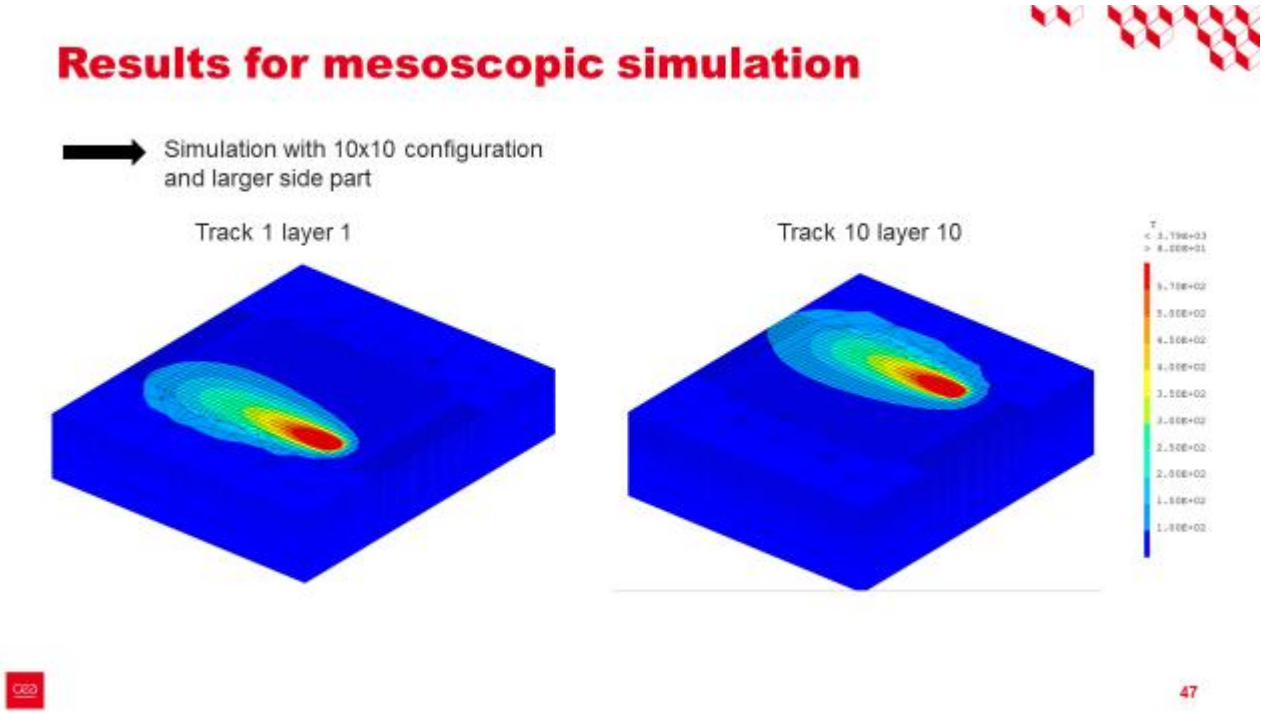
Results for mesoscopic simulation
Simulation with 10x10 configuration and larger side part
Track 1 layer 1
Track 10 layer 10
47

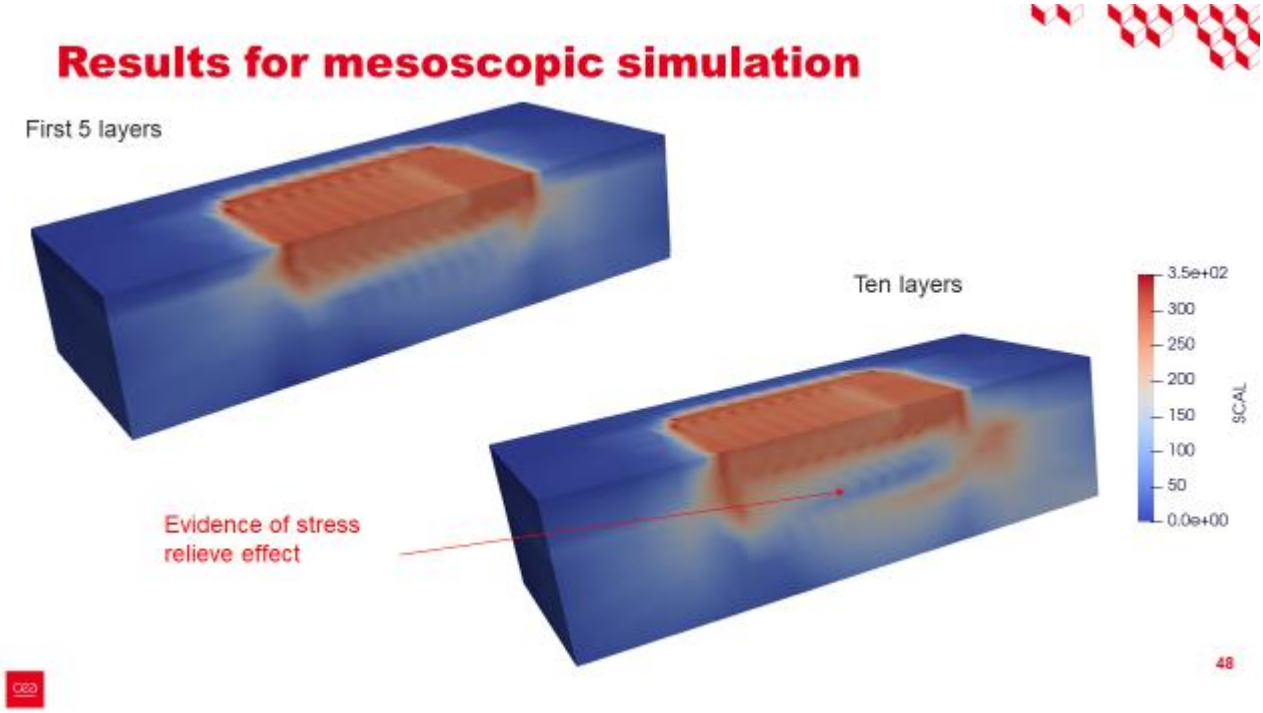
Results for mesoscopic simulation
First 5 layers
Ten layers
Evidence of stress relieve effect
3.5e+02
300
250
200
150
100
50
0.0e+00
SCAL
48

Results for mesoscopic simulation

- Residual stresses measurement will be clearly different between final surface and inside measurements (after rod cutting)
- Last surface measurement will give us more informations (and also will need less computed layers)

49

Geometric configuration for mesoscopic bi-material simulation

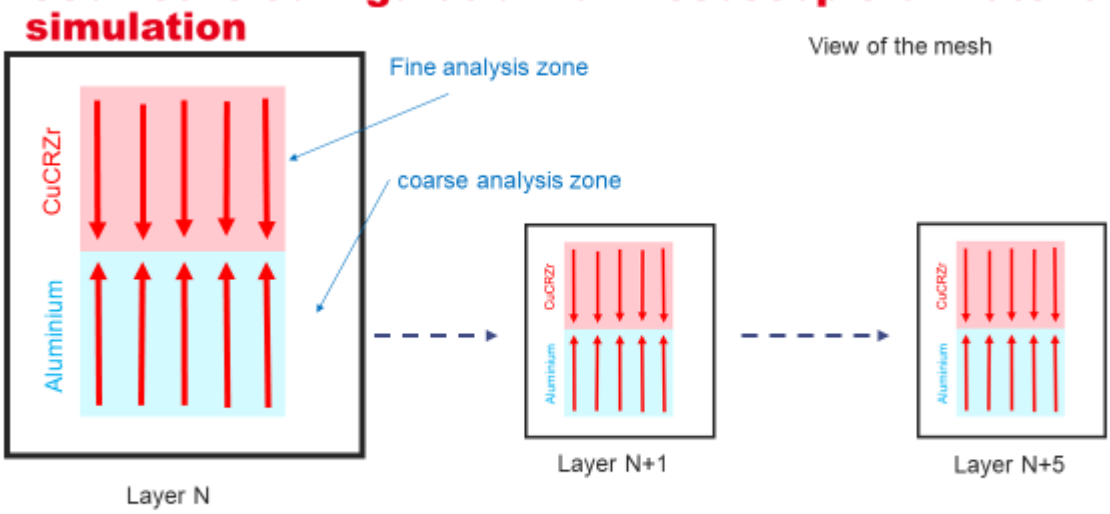

Solver configuration: only linear thermal model

Lasing strategy can be changed

50

Geometric configuration for mesoscopic bi-material simulation

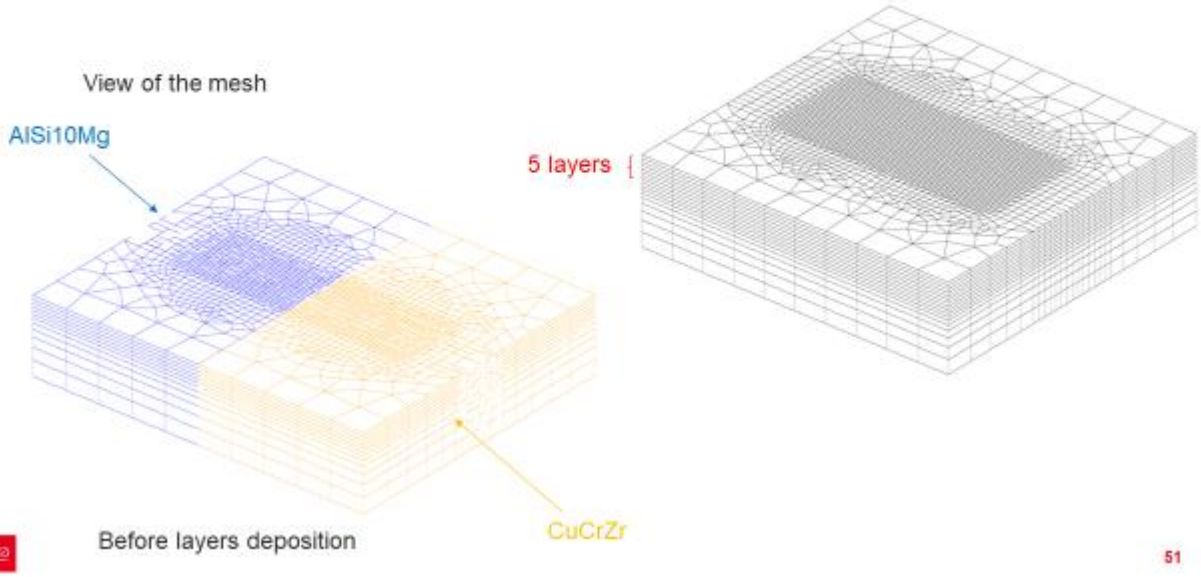

51

Geometric configuration for mesoscopic bi-material simulation

- Temperatures

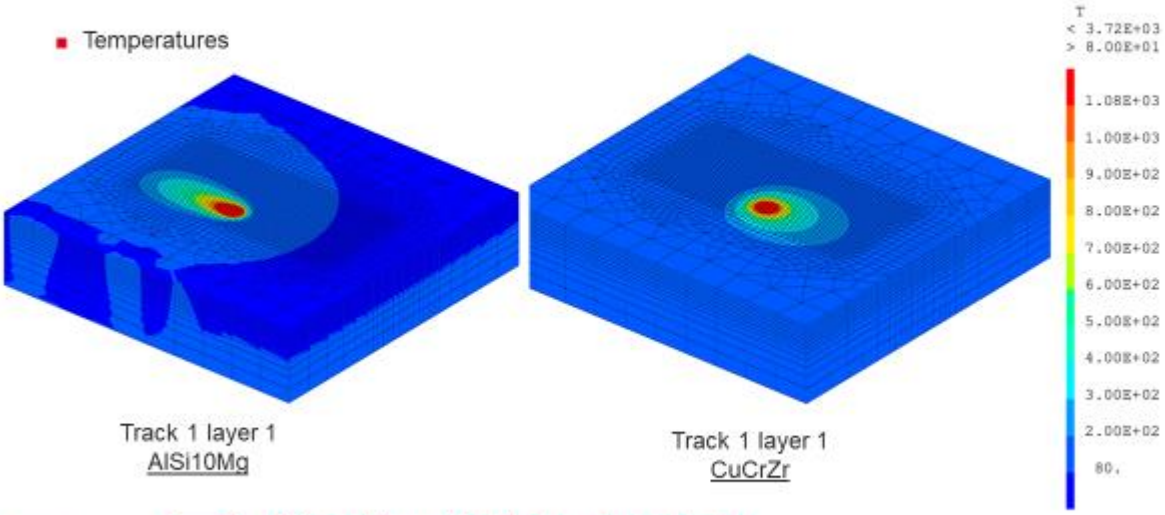

Different thermal field between two materials

52

Geometric configuration for mesoscopic bi-material simulation

- Temperature evolution at interface with layers

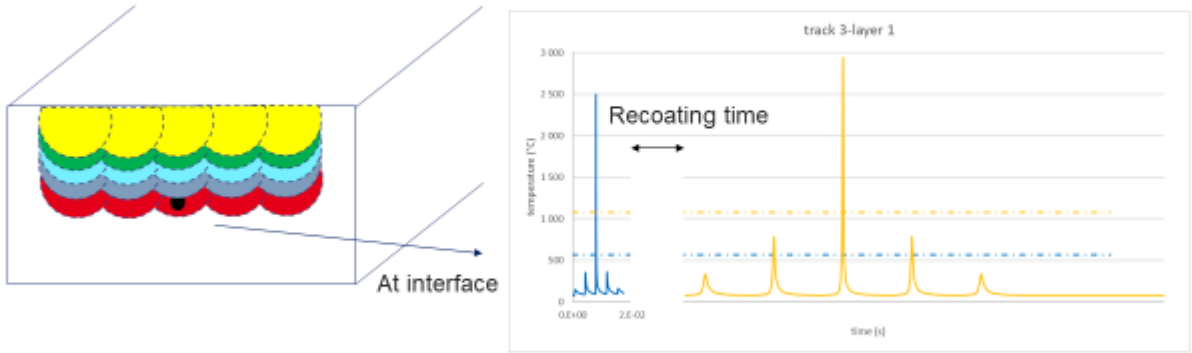

Added remelting induced by other side material lasing

53

Geometric configuration for mesoscopic bi-material simulation

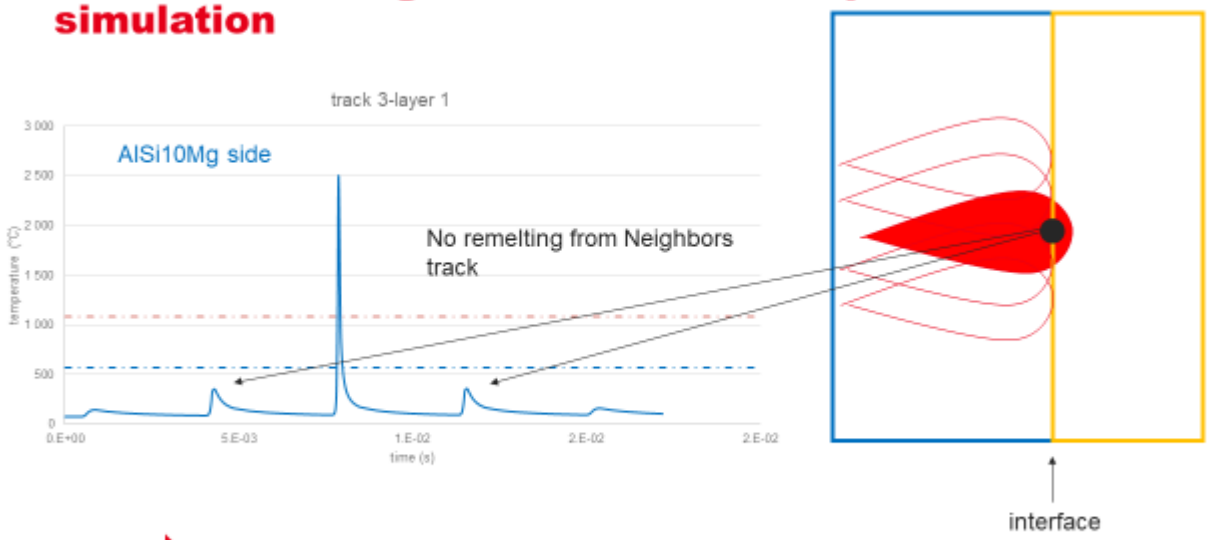

Basic perpendicular lasing strategy is not a good idea ☹

54

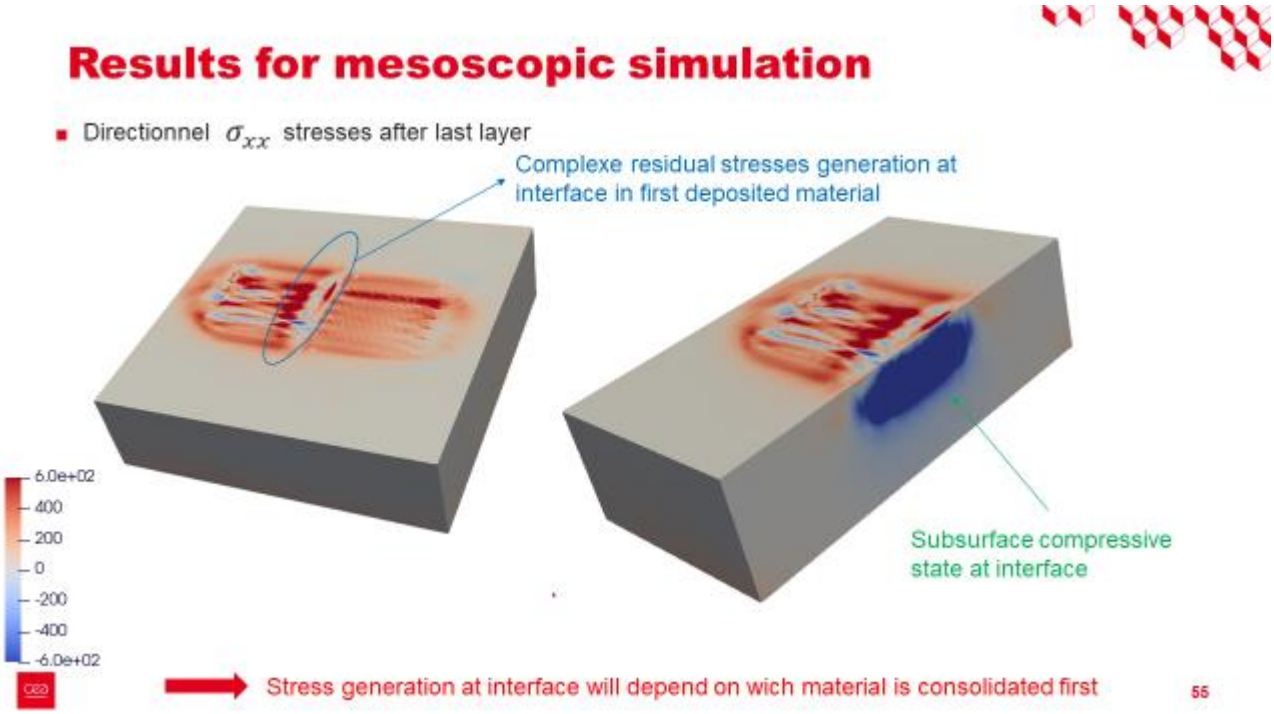
Results for mesoscopic simulation
Directionnel σ_{xx} stresses after last layer
Complexe residual stresses generation at interface in first deposited material
Subsurface compressive state at interface
6.0e+02
400
200
0
-200
-400
-6.0e+02
Stress generation at interface will depend on wich material is consolidated first
55

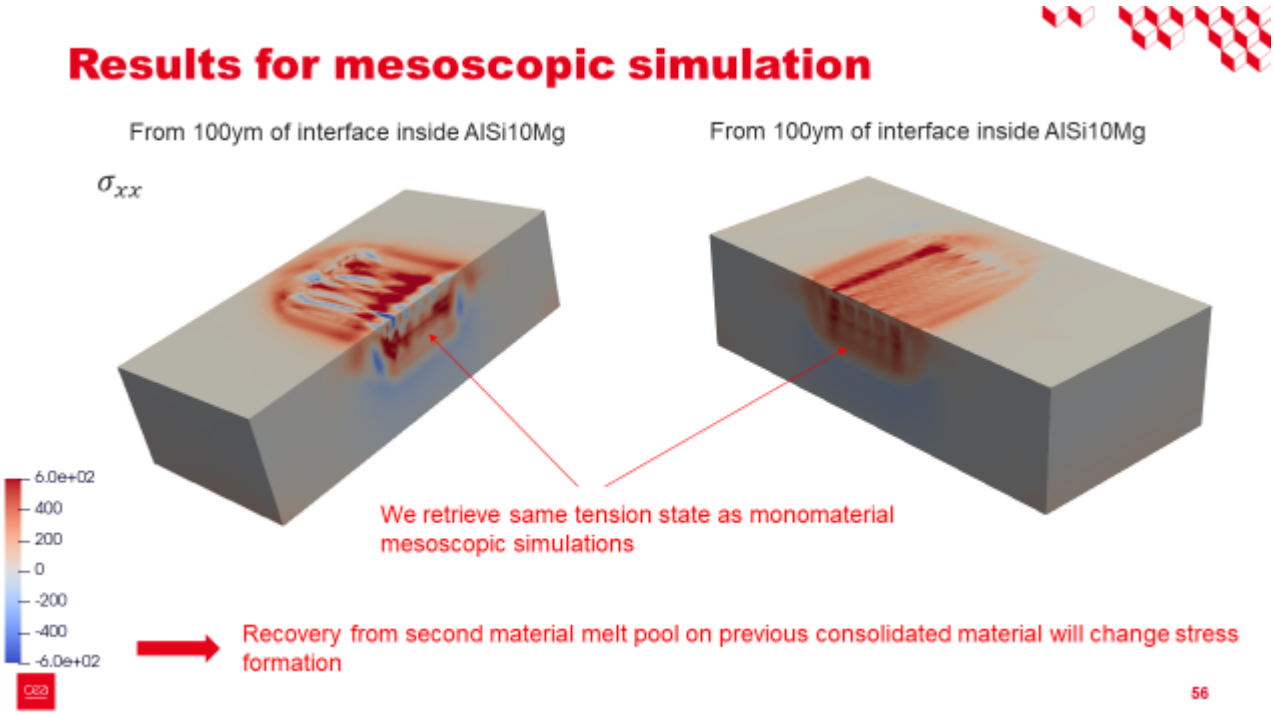
Results for mesoscopic simulation
From 100ym of interface inside AlSi10Mg
From 100ym of interface inside AlSi10Mg
σ_{xx}
We retrieve same tension state as monomaterial mesoscopic simulations
6.0e+02
400
200
0
-200
-400
-6.0e+02
Recovery from second material melt pool on previous consolidated material will change stress formation
56

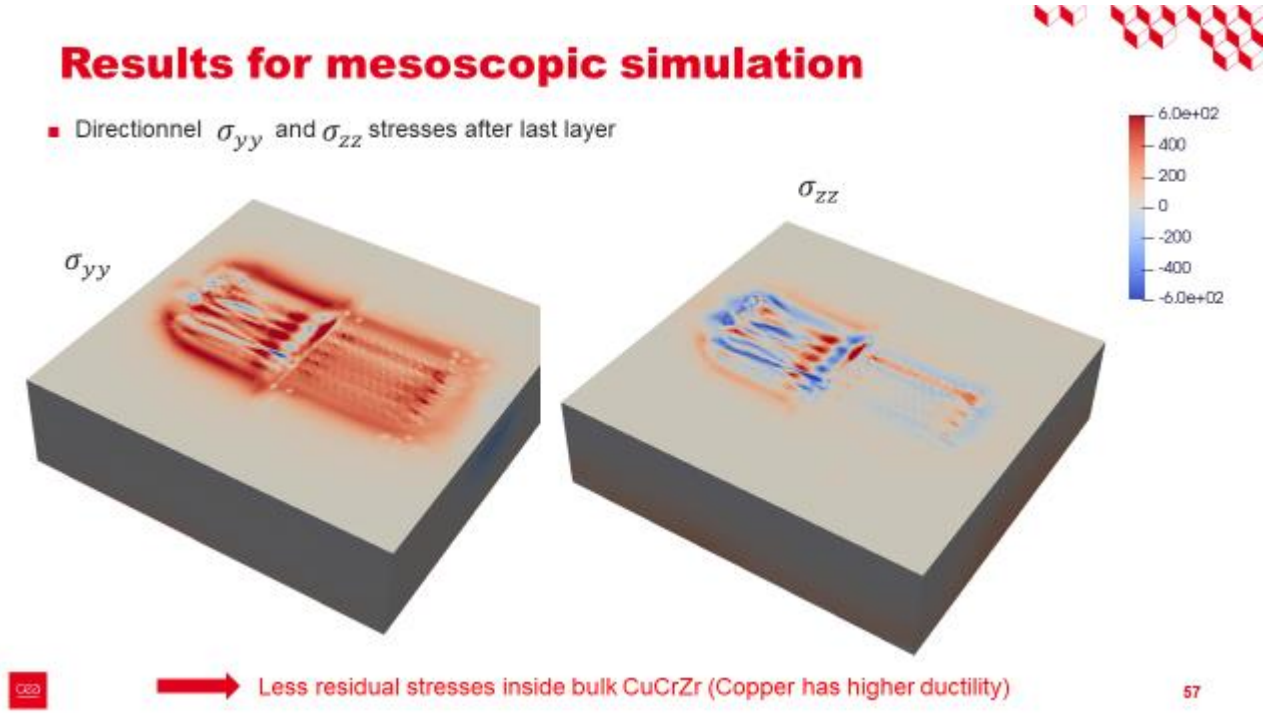
Results for mesoscopic simulation
Directionnel σ_{yy} and σ_{zz} stresses after last layer
σ_{yy}
σ_{zz}
6.0e+02
400
200
0
-200
-400
-6.0e+02
Less residual stresses inside bulk CuCrZr (Copper has higher ductility)
57

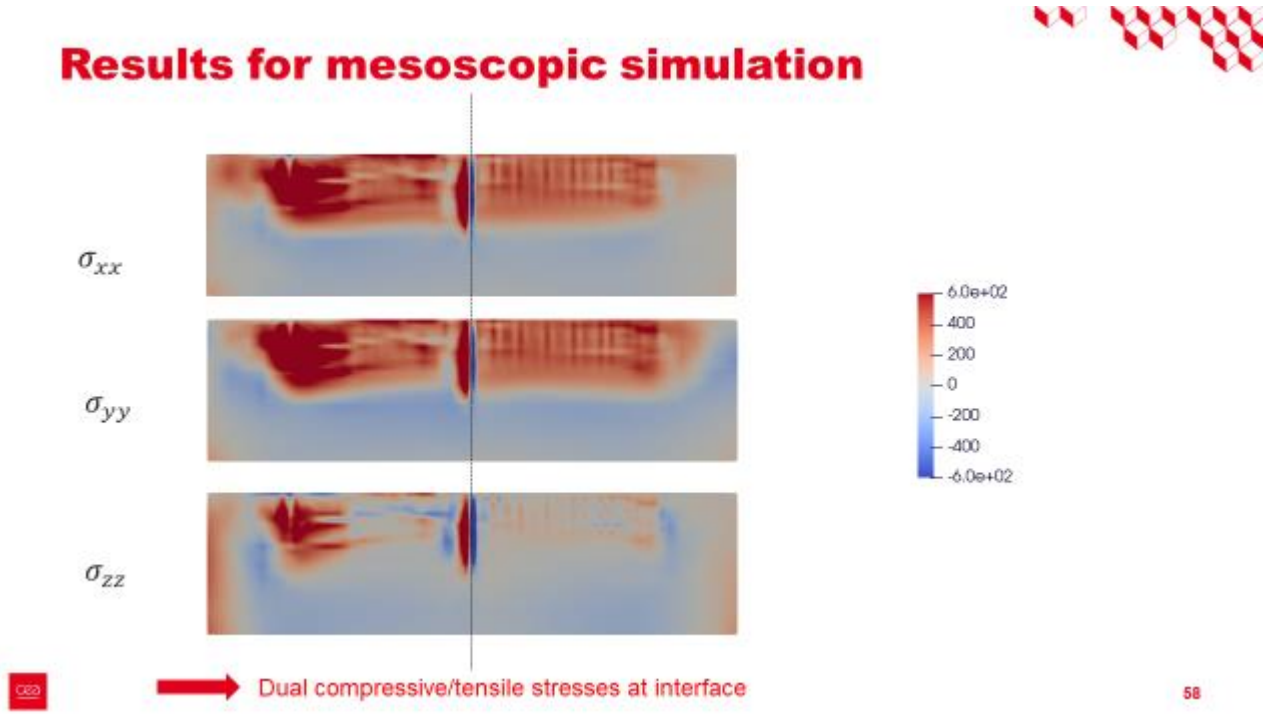
Results for mesoscopic simulation
σ_{xx}
σ_{yy}
σ_{zz}
6.0e+02
400
200
0
-200
-400
-6.0e+02
Dual compressive/tensile stresses at interface
58

Results for mesoscopic simulation

- Directionnel shear stresses after last layer

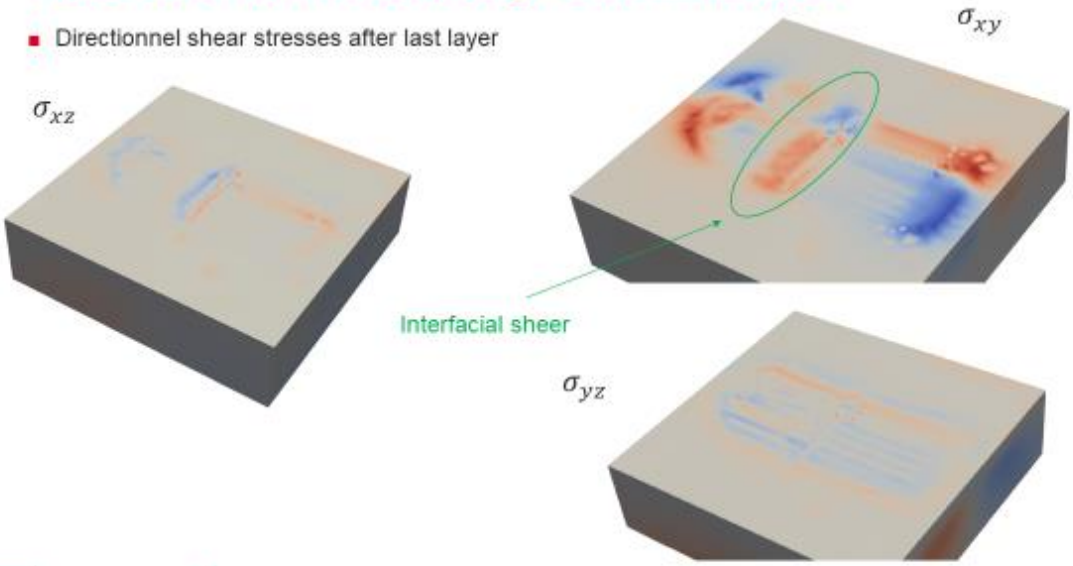

Shear along interface

59

conclusions

- We built a complete Finite Element thermomechanical model for mono/bimaterial L-PBF process at micro and meso-scale
- This model permit to access complete thermal history, in particular at interface for bimaterial configuration → input for diffusion calculations
- Computation of five deposited layers are sufficient to characterise near surface residual stresses
- A least 10 layers are necessary to characterise final residual stresses inside material
- In bimaterial configuration, complex residual stresses are observed near interface
- A better thermal solver is necessarry for that kind of simulations → models will be integrated into commercial F.E. software ANSYS©

60